Synchronizing ice-core and U/Th time scales in the Last Glacial Maximum using Hulu Cave ^{14}C and new ^{10}Be measurements from Greenland and Antarctica

Giulia Sinnl[1], Florian Adolphi[2], Marcus Christl[3], Kees C. Welten [4], Thomas Woodruff[5], Marc Caffee[5], Anders Svensson[1], Raimund Muscheler[6] and Sune Olander Rasmussen[1]

[1] Physics of Ice, Climate, and Earth, Niels Bohr Institute, University of Copenhagen, Copenhagen, Denmark.

[2] Alfred Wegener Institute, Helmholtz Centre for Polar and Marine Research, Bremerhaven, Germany

[3] Laboratory of Ion Beam Physics, ETH Zurich, Zurich, Switzerland

[4] Space Sciences Laboratory, University of California, Berkeley, California, USA

[5] Department of Physics and Astronomy, Purdue University, West Lafayette, Indiana, USA

[6] Quaternary Sciences, Department of Geology, Lund University, Lund, Sweden

Correspondence to: giulia.sinnl@nbi.ku.dk

Abstract

Between 15 and 27 ka b2k (thousands of years before 2000 CE) during the last glacial, Greenland experienced a prolonged cold stadial phase, interrupted by two short-lived warm interstadials. Greenland ice-core calcium data show two periods, preceding the interstadials, of anomalously high atmospheric dust loading, the origin of which is not well understood. At approximately the same time as the Greenland dust peaks, the Chinese Hulu Cave speleothems exhibit a climatic signal suggested to be a response to Heinrich Event 2, a period of enhanced ice-rafted debris deposition in the North Atlantic. In the climatic signal of Antarctic ice cores, moreover, a relative warming occurs between 23 and 24.5 ka b2k that is generally interpreted as a counterpart to a cool climate phase in the Northern Hemisphere. Proposed centennial-scale offsets between the polar ice-core time scales and the speleothem time scale hamper the precise reconstruction of the global sequence of these climatic events. Here, we examine two new ^{10}Be datasets from Greenland (NorthGRIP) and Antarctic

(WDC) ice cores to test the agreement between different time scales, by taking advantage of the globally synchronous cosmogenic radionuclide production rates.

Evidence of an event similar to the Maunder Solar Minimum is found in the new ^{10}Be datasets, supported by lower-resolution radionuclide data from Greenland and ^{14}C in the Hulu Cave speleothem, representing a good synchronization candidate at around 22 ka b2k. By matching the respective ^{10}Be data, we determine the offset between the Greenland ice-core time scale, GICC05, and the WDC Antarctic time scale, WD2014, to be 125±40 years. Furthermore, via radionuclide wiggle-matching, we determine the offset between the Hulu speleothem and ice core time scales to be 375 years for GICC05 (75–625 years at 68% confidence), and 225 years for WD2014 (-25–425 years at 68% confidence). The rather wide uncertainties are intrinsic to the wiggle-matching algorithm and the limitations set by data resolution. The undercounting of annual layers in GICC05 inferred from the offset is hypothesized to have been caused by a combination of underdetected annual layers, especially during periods with low winter precipitation, and misinterpreted unusual patterns in the annual signal, during the extremely cold period often referred to as Heinrich Stadial 1.

1 Introduction

Well-dated paleoclimatic archives, such as ice cores or speleothems, are essential for reconstructing the mechanisms of past climate change. Independent chronologies for each climatic archive are necessary for studying the recorded signals and are determined via, for example, counting annual layers or based on U/Th measurements. However, the uncertainties of each time scale and a lack of matching horizons hamper the global comparison of climatic proxy records.

During the Last Glacial Maximum (LGM) the ice sheets were at their largest extent (defined as ca. 23.3-27.5 ka by Hughes & Gibbard, 2015, although other definitions exist) and extreme climatic shifts were recorded in the Greenland and Antarctic ice cores, as well as in Asian speleothems such as the ones from Hulu Cave, China (Wang et al., 2001). To advance our knowledge of the LGM as recorded in the archives, we need to estimate the leads and lags between these shifts, but a climatic synchronization is not always possible and not free of interpretation caveats. A lack of secure tie points over the LGM by most synchronization studies (Svensson et al., 2020; Corrick et al., 2020; WAIS project members, 2015) makes the reconstruction of a global sequence of events difficult to assess.

In Greenland ice cores, the water stable isotope data (e.g. $\delta^{18}O_{ice}$) records two unusually short and small Greenland interstadials, GI-2.1 and 2.2 (Rasmussen et al., 2014), briefly interrupting the long

cold period formed by the two Greenland stadials GS-2 and GS-3 (Fig. 1a). Despite other periods of interstadial climate conditions being recorded widely across the Northern hemisphere, there is no counterpart of the brief GI-2.1 and 2.2 in the Hulu $\delta^{18}O_{calcite}$ (Fig. 1b), which hampers the comparison of Greenland ice cores and Asian speleothems.

Around the same time, the $\delta^{18}O_{ice}$ in several Antarctic ice cores reaches a maximum (AIM-2; EPICA Community Members, 2006), interrupting a warming trend (Fig. 1c). Greenland and Antarctic $\delta^{18}O_{ice}$ records are hypothesized to be coupled by the bipolar seesaw mechanism (Stocker & Johnsen, 2003), by which a Greenlandic transition to an interstadial will initiate cooling in Antarctica with a small delay. According to the current chronologies, however, the onset of the Antarctic cooling, i.e. the peak of the AIM-2, leads the onset of the GI-2.2 by about 260 years. The average delay, or signal transmission time, from the North Atlantic to the Antarctica is estimated to be 1 to 2 centuries, as shown by ice core measurements (Svensson et al., 2020; WAIS project members, 2015) and in line with modelling experiments (Pedro et al., 2018), but the lead-lag dynamic appears to be reversed for AIM-2.

During GS-2 and GS-3, at least two massive discharge events of icebergs from the Laurentide ice sheet were inferred from the ice-rafted debris content of North Atlantic marine sediments, defining the occurrence of the Heinrich Events 1 and 2 (HE-1 and HE-2; Bard et al., 2000; Peck et al., 2006), which are each now thought to consist of 2 pulses. Heinrich events occurred during Greenland stadials and added a large amount of freshwater to the surface ocean, likely causing an extreme shutdown of the Atlantic overturning meridional circulation (AMOC) and, thereby, prolonged climatic conditions of severe cold (McManus et al., 2004). The term Heinrich stadial (HS) is often used to indicate the period affected by the Heinrich events.

Signatures of climatic change likely related to HS-1 and HS-2 are recorded in the $\delta^{18}O_{calcite}$ of the Hulu speleothems (Fig. 1b; Cheng et al., 2018), but no counterpart is found in the Greenland $\delta^{18}O_{ice}$. Possible reasons include that the high-latitude areas around the ice sheet were not strongly affected by the cooling or that the isotopes reacted non-linearly (Guillevic et al., 2014). It has also been suggested that, during HS-1, changes in the precipitation seasonality influenced the annual mean $\delta^{18}O_{ice}$ in a way that obscured the relation of $\delta^{18}O_{ice}$ and annual average temperatures (He et al., 2021). This may also apply to HS-2. While $\delta^{18}O_{ice}$ does not show a clear imprint of the Heinrich events, Greenland ice-core calcium data show two periods of heightened concentration during GS-3 (Fig. 1a; Rasmussen et al., 2014) that could be related to atmospheric reorganization around HE-2 (Adolphi et al. 2018), although there is debate about this attribution (Hughes & Gibbard, 2015). Since mineral

dust aerosols in Greenland originate mostly from the Eurasian continent (Schüpbach et al., 2018) and the dust record therefore should reflect climate variability in Asia, Dong et al. (2022) synchronized the youngest Greenland calcium peak to the HS-2 signal of an Asian speleothem (Cherrapunji, India). Based on the assumption of synchronous climate signals, they inferred a multi-centennial dating offset between the GICC05 ice-core time scale and the U/Th-dated speleothem record, that is consistent with earlier estimates based on cosmogenic radionuclides (Adolphi et al. 2018).

In addition to the Antarctic warming indicated by AIM-2, an abrupt rise of methane levels (Fig. 1c) indicates a likely response of the tropical methane emission sources to a period of climate change (Rhodes et al., 2015), which is suggested to correspond to HS-2. The phasing of the methane signal and the Heinrich stadial is still unresolved because of possible offsets in the respective chronologies.

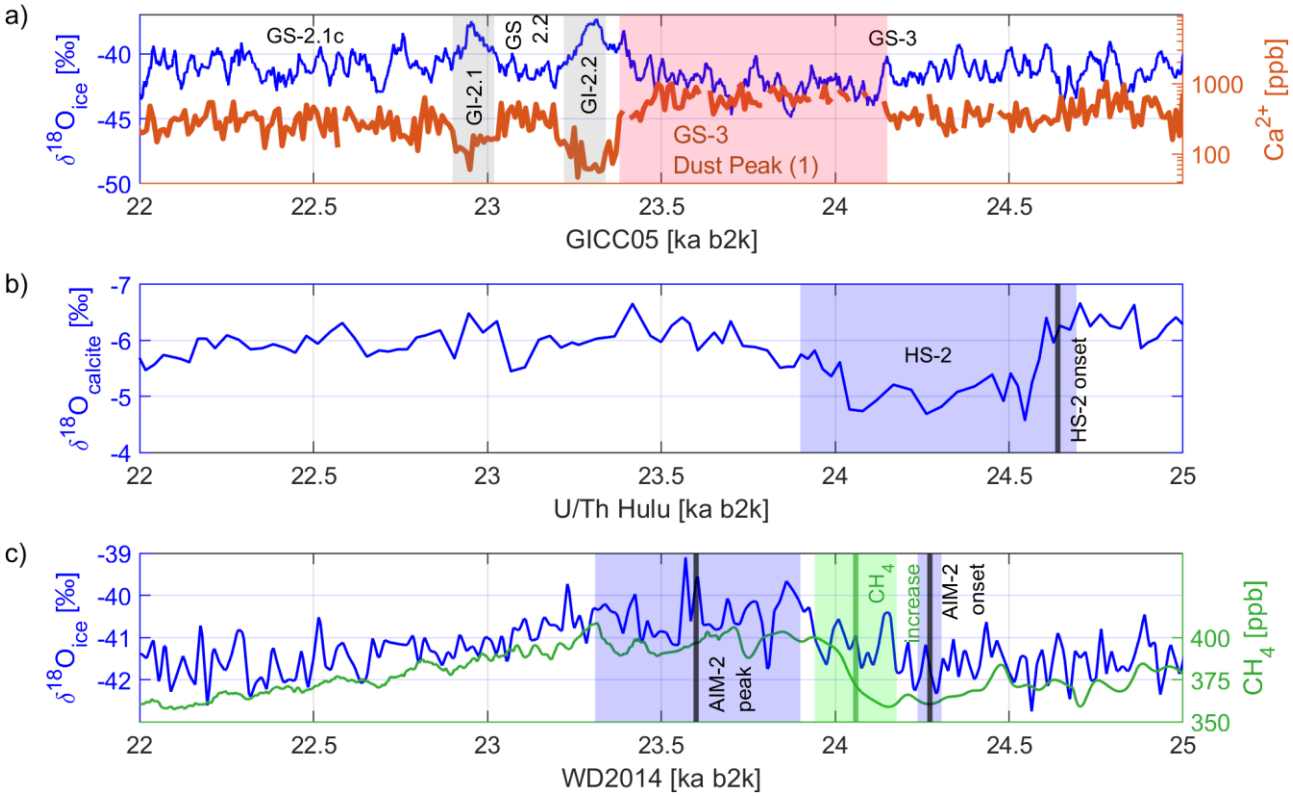

Figure 1 Climate signals on their original time scales. The time direction is from right to left. The references to all datasets are summarized in Table 1. Notice the relative position of onsets and terminations of the climate shifts. a) Greenland stable oxygen isotopes (GRIP) and calcium (log scale, NorthGRIP), showing the alternating signals of interstadials (GI) and stadials (GS), as defined by Rasmussen et al. (2014), and the dust peak during GS-3. b) Hulu Cave stable oxygen isotopes, on a reversed y-axis, showing the cold phase attributed to HS-2. c) Antarctic (WD ice core) stable oxygen isotopes showing the Antarctic Isotope Maximum 2 (AIM-2; EPICA community members, 2006), and the methane record showing a rapid increase.

The unclear causal relationships between the mentioned signals challenge the interpretation of the climate dynamics of the LGM. The time scale uncertainties of each archive, in the order of centuries

for the ice-core chronologies (Svensson et al., 2008; Sigl et al., 2016), mask any absolute inference of the climatic leads and lags. Non-climatic synchronization horizons such as volcanic eruptions or solar events are needed to obtain solid estimates of the relative time scale offsets. For example, Svensson et al. (2020) compared the two layer-counted polar chronologies GICC05 (Greenland ice core chronology; Svensson et al., 2008) and WD2014 (WAIS Divide chronology; Sigl et al., 2016) via bipolar volcanic tie points. They found a negligible offset at 16 ka and only 80 years at 24.6 ka. However, they lack tie points within this entire interval.

Traces of cosmogenic radionuclides (e.g., ^{14}C and ^{10}Be) allow for global synchronizations because of their common production history and widely recorded signals. So far, the only radionuclide-based tie point in the LGM between ice-core and Hulu Cave records was found by Adolphi et al. (2018). Around 22 ka, they measured an offset of 550 years (95% probability interval: 215-670 years) between GICC05 and the Hulu time scale, the latter being oldest.

This offset is unexpected considering the good agreement between the two chronologies measured both before and after the LGM; the climate synchronization between speleothems and GICC05 by Corrick et al. (2020) found small offsets of 4 years at GI-1 (15 ka) and of 92 years at GI-3 (27.5 ka). Nonetheless, the climatic synchronization by Dong et al. (2022) suggests that GICC05 is too young compared to the Cherrapunji speleothem U/Th ages and estimates the offset to 320 years (with a 2σ-uncertainty of 90 years) around 24.5 ka. In addition, the WD2014 and Hulu timescales are offset by 167 years around GI-3 (Sigl et al., 2016), suggesting that the Antarctic ice core chronology may also be diverging from U/Th ages.

In this study, to better determine the sequence of events during the LGM, we aim at establishing strong ties between the three chronologies: GICC05, WD2014, both dated by annual layer counting, and Hulu Cave, dated by U/Th measurements. Since the WD2014 chronology in the LGM was never compared against the Hulu and GICC05 chronologies, new Antarctic ^{10}Be measurements are needed to fill the gap. Further, new ^{10}Be measurements from Greenland are needed to strengthen the statistical significance of the 22-ka tie point by Adolphi et al. (2018), which presents a low signal-to-noise ratio. The Hulu cave $^{14}C_{calcite}$ and $\delta^{18}O_{calcite}$ measurements were updated in recent years (Cheng et al., 2018) and directly included in the radiocarbon calibration curve (IntCal20; Reimer et al., 2020), used to date radiocarbon from organic samples worldwide. We therefore aim to evaluate the tie point by Adolphi et al. (2018) using new measurements of ^{10}Be and the recent $^{14}C_{calcite}$. We will use a combination of carbon-cycle modelling and statistical wiggle-matching (Siegenthaler, 1983; Adolphi & Muscheler, 2016) to directly compare proxy records from both polar ice sheets and the Hulu cave.

In this work, we confirm the existence of centennial offsets in the LGM between the three chronologies and we position the mentioned global climatic shifts in relation to each other. The question of why chronological offsets quickly develop remains open, but we suggest that difficulties with annual-layer identification in the very cold parts of the last glacial are the likely source of the observed offsets.

2 Data and Methods

In this study, we aim at comparing the new cosmogenic radionuclide data with other datasets from Greenland, Hulu Cave, and Antarctica. We also analyze water stable isotope, methane, and calcium data to assess climatic changes. We summarize the relevant datasets, age resolutions, and citations in Table 1. In this work, we refer to years b2k because they are commonly used for the GICC05 time scale; when necessary, we have converted from years BP (before 1950 CE) by adding 50 years.

Table 1 Datasets used in this study. Age resolutions represent the period 20 to 25 ka b2k. For the Hulu Cave, $^{14}C_{calcite}$ data from two speleothems from the cave, labelled H82 and MSD, were published in two separate studies.

Dataset	Location	Proxy	Avg. Age Res., years	Reference
NorthGRIP	75°10′N 42°32′W	^{10}Be	10	This study
		Ca^{2+}	20	Erhardt et al., 2021
		$\delta^{18}O_{ice}$	10	NorthGRIP members, 2004
GRIP	72°58′N 37°64′W	^{10}Be	27	Yiou et al., 1997; Muscheler et al., 2004
		$\delta^{18}O_{ice}$	10	Johnsen et al., 1997
GISP2	72°36′N 38°30′W	^{10}Be	162	Finkel & Nishiizumi, 1997
		$\delta^{18}O_{ice}$	10	Stuiver & Grootes, 2000
WDC	79°46′S 112°08′W	^{10}Be	67	This study
		$\delta^{18}O_{ice}$	10	Jones et al., 2017
		Non-sea-salt-Sulfate (nssS)	1	Buizert et al., 2018
Hulu Cave	32°30′N 119°10′E	$^{14}C_{calcite}$	271	H82: Southon et al., 2012
			124	MSD: Cheng et al., 2018
		$\delta^{18}O_{calcite}$	70	H82: Wang et al., 2001; Wu et al. 2009
			31	MSD: Cheng et al., 2016

2.1 Preparation and measurement of the NorthGRIP samples

The 322 new Greenland ^{10}Be measurements were performed at ETH Zurich on samples from the NorthGRIP ice core between 1726.45 m and 1816.51 m depth, which according to GICC05 correspond to ages between 20,039 to 24,774 years b2k (Andersen et al., 2006). The samples have a variable temporal resolution between 7.5 years and 14 years with some smaller gaps (see Methods Appendix, sec. 8.2) and are the so-far best-resolved available radionuclide dataset for the LGM. The

extraction of ^{10}Be followed protocols by Nguyen et al. (2021), see Methods Appendix, sec. 8.3. The measured ^{10}Be concentrations are shown in Fig. 2a.

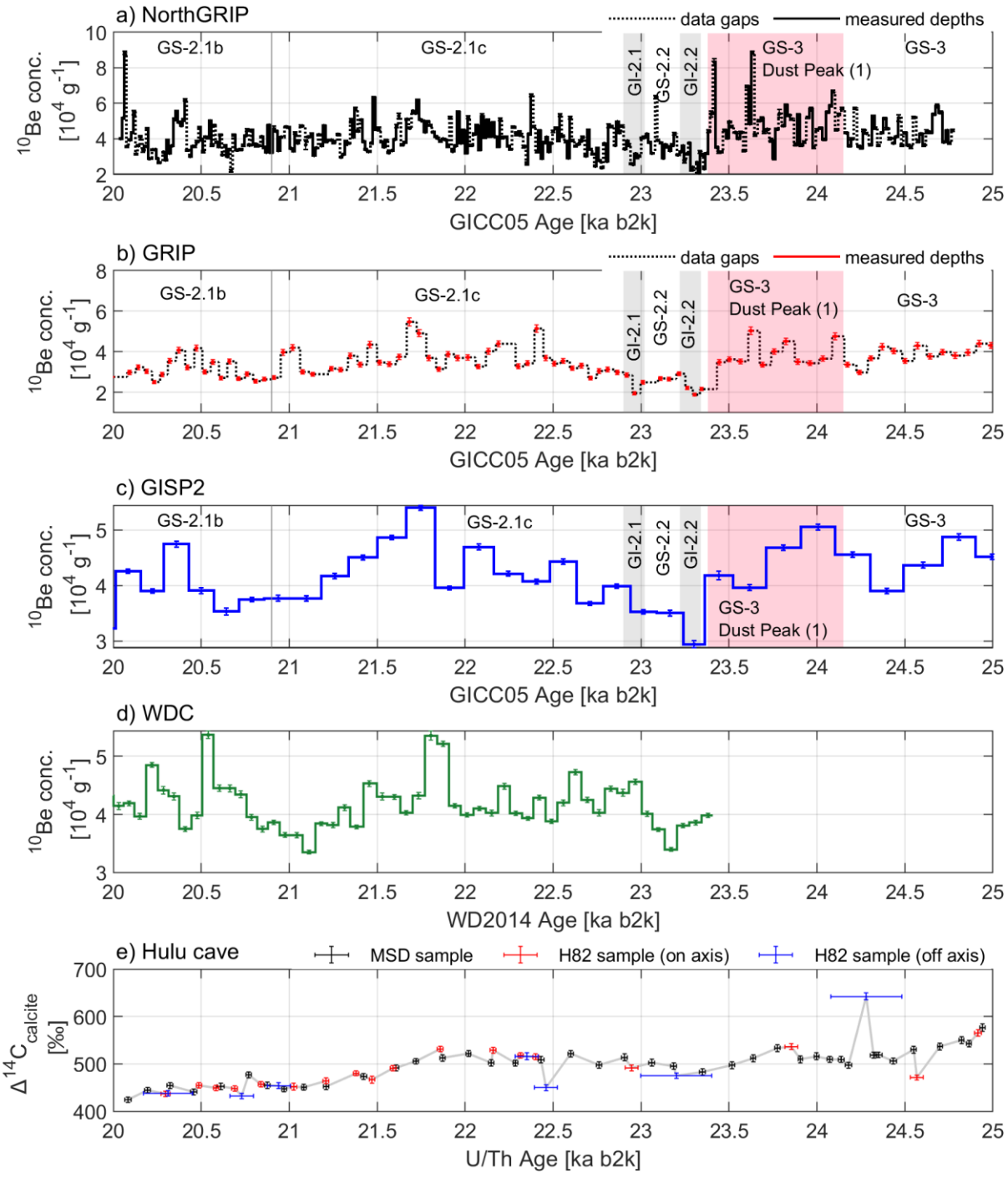

Figure 2 Cosmogenic radionuclide data used in this study (see Table 1 for references). On the GICC05 time scale: ^{10}Be concentrations in (a) NorthGRIP, (b) GRIP, and (c) GISP2. Dotted lines in the GRIP data indicate discontinuities between every 55-cm resolved sample. On the WD2014 time scale: (d) WDC ^{10}Be concentrations. On a U/Th-based time scale: (e) Hulu Cave $\Delta^{14}C_{calcite}$ data as reported in three separate datasets. In the following, we exclude the off-axis H82 measurements (blue), as they show more outliers and wider dating uncertainties.

2.2 Preparation of the WDC samples and measurement

A total of 73 samples in the WAIS Divide 06A ice core (WDC-06A), from 2453 to 2599 m depth, were analysed for ^{10}Be concentrations at Purdue University. These samples represent continuous ice-core sections with a cross-section of ~2 cm^2, varying from 1.89 to 2.12 m in length (~60-75 years of snow accumulation per sample). The extraction followed established protocols (Woodruff et al. 2013), see Methods Appendix sec. 8.1 for more details. Fig. 2d shows the measured WDC ^{10}Be concentrations.

2.3 Conversion of ^{10}Be concentrations to fluxes

To account for the first-order correction of climatic influences on the ^{10}Be signal (Adolphi et al., 2018), we need to convert the ^{10}Be concentrations to fluxes, which requires knowledge of accumulation rates (see Methods Appendix sec. 8.3). Accumulation rates for the ice cores are reconstructed using the annual layer thicknesses and an appropriate model for the layer thinning. The thinning in the LGM portion of the ice cores can be approximated by a linear function of depth, although there may be uncertainties that relate to the time scale itself.

For the NorthGRIP ice core, the layer thickness was directly derived from the annual layers of the GICC05 (Andersen et al., 2006), while the thinning was modelled by Johnsen et al. (2001). For WDC, the accumulation rate (Fudge et al., 2016) was inferred from the WD2014 layer thicknesses and modelled thinning (Buizert et al., 2015). The new ^{10}Be fluxes are shown in Fig. 2, together with the modelled accumulation rates. The fluxes of NorthGRIP are clearly less affected by changing snow accumulation rates than 10Be concentrations, as seen in the absence of GI/GS-related changes in 10Be, which is similar to other Greenland ice core 10Be-records (e.g., Muscheler et al. 2004). To show that the flux conversion largely removes the climatic influence on ^{10}Be deposition in Greenland, we checked the residual correlations with other climate proxies in Fig. S3.

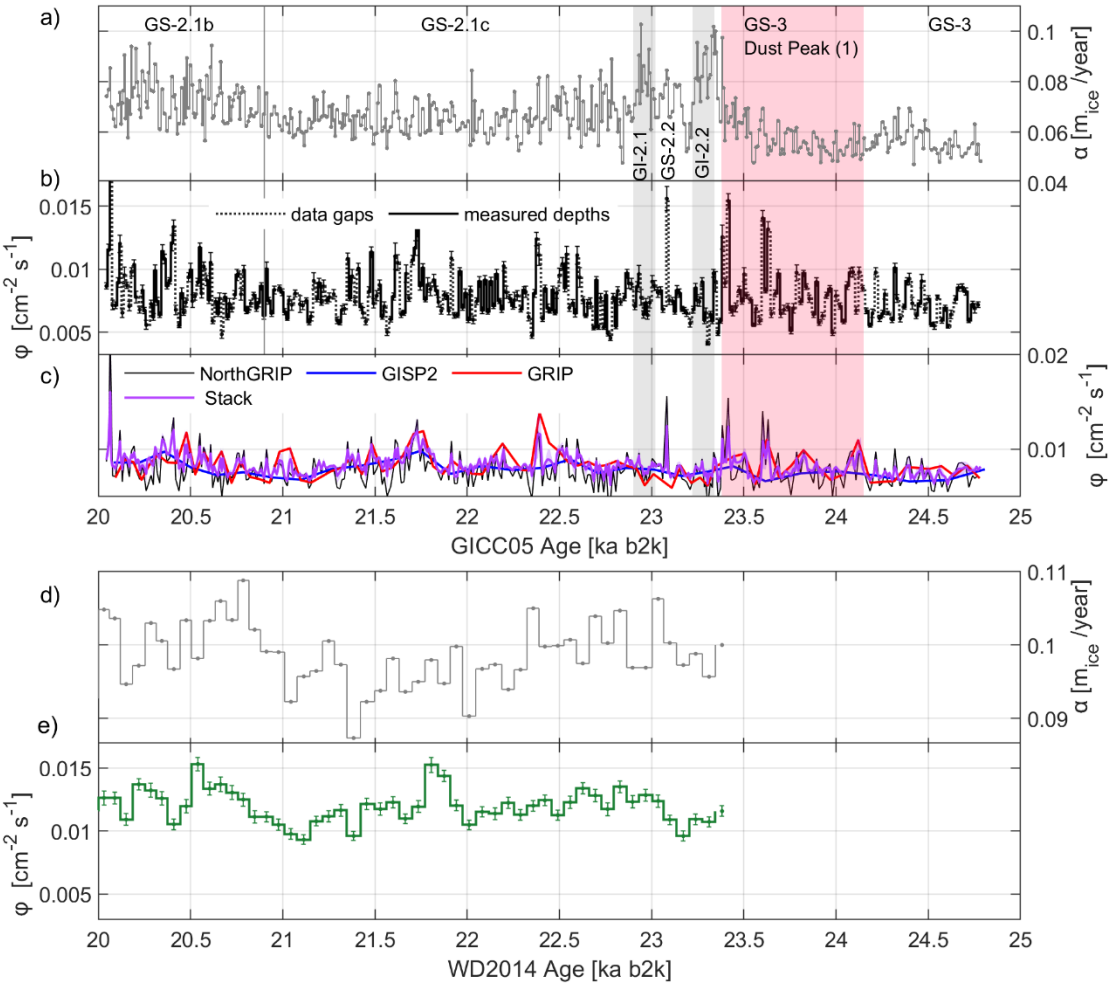

Figure 3 (a) The accumulation rate of NorthGRIP, down sampled to the same depth resolution of each ^{10}Be data point. (b) The ^{10}Be fluxes of NorthGRIP have an average of 0.008 ± 0.002 atoms cm^{-2} s^{-1}. (c) Stack of the fluxes of the three Greenland ice cores, on 10-year resolution. (d) The published accumulation rate of WDC (Fudge et al., 2016), down-sampled to the age resolution of the ^{10}Be concentrations. (e) The ^{10}Be fluxes of WDC average at 0.011 ± 0.001 atoms cm^{-2} s^{-1}, higher than in Greenland, either because of depositional differences between the poles (Heikkilä et al., 2013) or because of accumulation rate inaccuracies.

Over the LGM, the GRIP and GISP2 ice cores were tied to NorthGRIP by identification of volcanic tie points and biomass burning events, and GICC05 was extended to these ice cores by interpolation (Rasmussen et al., 2008; Seierstad et al., 2014). The annual layer thickness is thus less certain for GRIP and GISP2 and, due to a scarcity of volcanic tie points across the LGM, the accumulation difference across the short interstadials GI-2.1 and 2.2 may be at risk of misinterpretation. We used the most recent versions of GRIP and GISP2 thinning functions to calculate fluxes (Lin et al., 2021; Hvidberg et al., 1997), but we actively modified the accumulation history using new ^{10}Be tie points, as delineated in section 3.2.

The ^{10}Be measurements recently performed in the LGM on the NEEM ice core (Zheng et al., 2021) have similar resolution as the GISP2 data set. The NEEM data set does not resolve the ^{10}Be features we are studying well, and we therefore do not consider this dataset further on.

Finally, an average of the ^{10}Be fluxes of the three Greenland ice cores was calculated by stacking the NorthGRIP, GRIP and GISP2 fluxes, using Monte-Carlo bootstrapping (Adolphi et al., 2018). The assumption behind averaging fluxes is that local accumulation effects are mostly removed by the conversion to fluxes and that the climatic effects on ^{10}Be deposition are the same over Greenland. For each iteration, three of the data series are selected with resampling, each dataset is perturbed within its uncertainties, and averaged. The stack is shown in Fig. 3c.

2.4 Carbon cycle modelling and uncertainties

The interaction of galactic cosmic rays (GCRs) with the atmospheric parent atoms (N, O) of ^{10}Be and ^{14}C is modulated by the time-varying helio- and geomagnetic fields. The radionuclides recorded in climatic archives ideally show synchronizable features in their production history (Steinhilber et al., 2012; Adolphi et al., 2018). The ^{14}C atoms enter the carbon cycle, which causes delay and smoothing of the atmospheric ^{14}C concentration relative to the production signal. However, the connection with the rapidly deposited ^{10}Be in ice cores (1-2 years depositional delay; Raisbeck et al., 1981) can be made using a carbon-cycle model. Here, the box-diffusion model by Siegenthaler (1983) is applied to derive the atmospheric Δ^{14}C signal, i.e. the decay and fractionation-corrected ratio of ^{14}C/^{12}C relative to a standard (Stuiver & Pollach, 1977), from the measured ice-core ^{10}Be. This model was used extensively in works by Muscheler et al. (2000, 2004, 2009, 2014) and Adolphi et al. (2014, 2016, 2018).

We assume here that any variations of ^{10}Be in ice cores can be converted to a global ^{10}Be production rate, proportional to the global ^{14}C production rate. This assumption may, however, lead to uncertainties. For example, changes in the balance between wet and dry deposition or changes in the transport of ^{10}Be to the ice sheet are possible factors that might alter the signal recorded in ice cores from the true production rate.

The ice-core ^{10}Be is normalized relative to its mean, amplified by 20% (as estimated below), and provided as input signal to the model. The model should run with parameters that best represent the state of the carbon cycle and its changes through time, with the assumption that any remaining variability will be related purely to production effects. However, as we do not know these carbon cycle changes well enough, we keep in mind, however, that the measured ^{14}C may have been affected

by changes in the carbon cycle that are not considered in the model, adding additional signals that are not related to production rate changes.

In the period 20-25 ka b2k, the Hulu Cave $\Delta^{14}C_{calcite}$ is about 500‰ (Fig. 2e), which is higher than early Holocene values, which are below 200‰ (Reimer et al., 2020). These higher values may be related to one or more of the following factors: a lower ocean diffusivity during the LGM or any process that similarly reduces the carbon uptake by the ocean (Muscheler et al., 2004), a lower atmospheric ^{12}C inventory resulting in higher $^{14}C/^{12}C$ ratios (Köhler et al., 2022), or a weaker geomagnetic field. For instance, Muscheler et al. (2004) expect the ^{10}Be production rates in the LGM to have been about 20% higher than today, due to the lower geomagnetic field intensity during the LGM.

To determine the most appropriate model parameters, we repeat the calibration by Adolphi et al. (2018) around the Laschamps geomagnetic excursion at 41 ka b2k, since the available ^{14}C data has been updated since then (Reimer et al. 2020). We run the model with different ocean ventilation values (Fig. S1), finding that, for values of ocean diffusivity between 25-40% of the pre-industrial Holocene value, the modelled $\Delta^{14}C$ match the IntCal20 data best. This is in agreement with Muscheler et al. (2004) who performed a time-dependent adjustment of the ocean diffusivity parameter between 10-25 ka b2k. In their study, the LGM ocean diffusivity was set to ~1000 m^2/yr, about 25% of the pre-industrial Holocene value.

In summary, we find that a 20% production rate amplification of the normalized ^{10}Be and an ocean diffusivity of 25% of the pre-industrial Holocene value produce modelled outputs of about 500‰, in agreement with the Hulu-Cave measurements, although the model fails to capture the decreasing trend. We note that this is not necessarily a realistic parametrization of the state of the carbon cycle, but it allows us to match some of the main features seen in the data. We associate no uncertainty with the model parameters since no setup realistically explains all the $\Delta^{14}C_{calcite}$ features.

To compare the measured and the modelled $\Delta^{14}C$, in this study we will make use of linear detrending, as this largely removes the systematic offsets associated with the unknown carbon cycle history and inventories. The detrending is performed by, first, selecting data in the 20-25 ka b2k timeframe and, then, using the Matlab function “detrend”, which subtracts the best-fit line from the data. Some residual effect of the parametrization is observable in the amplitude of detrended $\Delta^{14}C$, but not in the timing of the changes, which is most important here.

2.4.1 Sensitivity tests: ocean diffusivity changes, accumulation rate uncertainties, measurement uncertainties.

To provide an uncertainty boundary for the detrended modelled $\Delta^{14}C$ curves, we performed three separate sensitivity test. As a first test, we investigated how short-term changes in the ocean diffusivity affect the modelled output, because during the LGM there likely have been changes in the carbon cycle around the GIs and the HS-2 (Bauska et al., 2021).

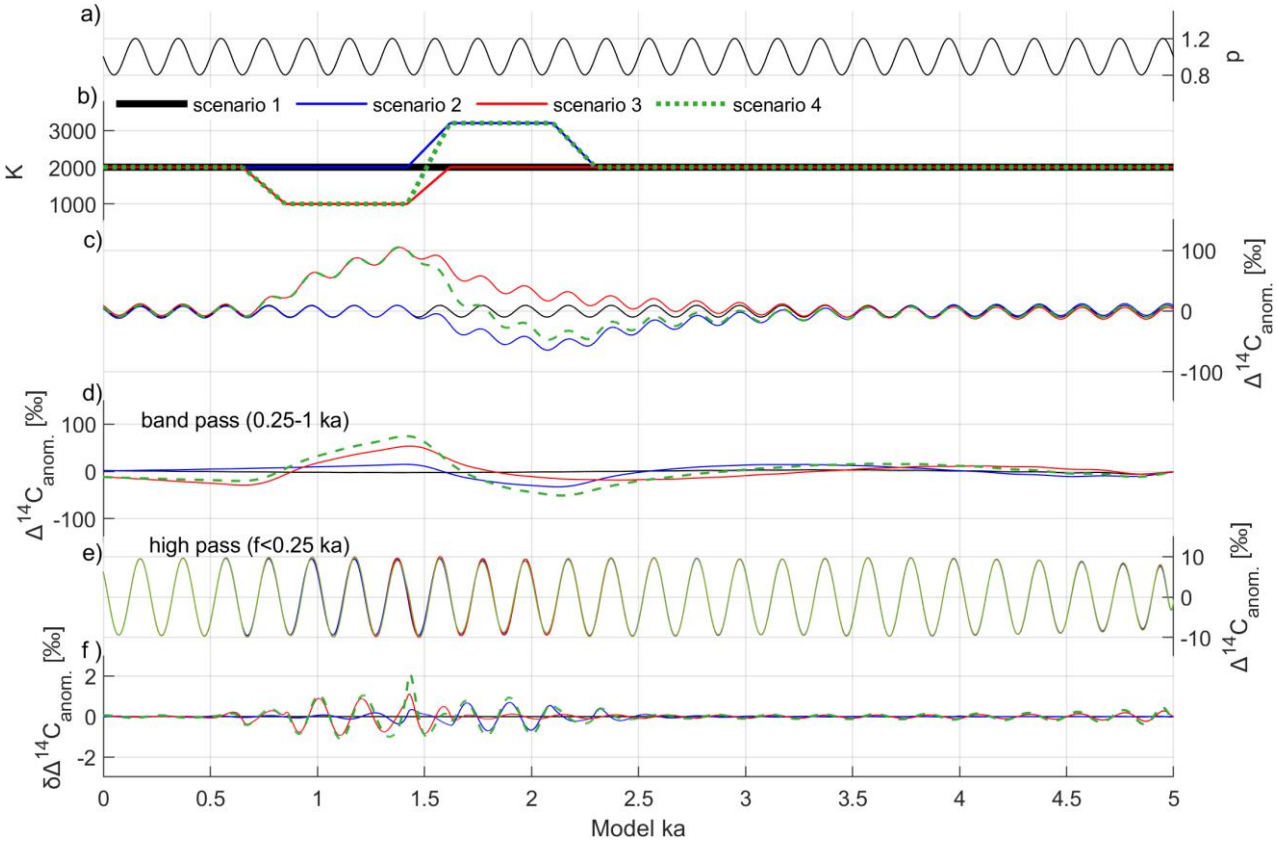

Figure 4 Sensitivity tests for time-dependent ocean diffusivity changes.
(a) Normalized production rate input shaped as a periodic wave with an amplitude of ±25% and a period length of 200 years, broadly consistent with typical solar de-Vries cycle variability observed in ^{10}Be (e.g. Wagner et al., 2001). (b) Scenarios of ocean diffusivity, as described in the text. (c) Model output, after linear detrending. (d) Long-term variations of the output (band-pass filtered with periodicity 250-1000 years). (e) High-pass filtered output, up to 250-year periodicity, having amplitudes of around 20‰. (f) Differences of the high-pass filtered curves in (e) between the control scenario 1 and the other three scenarios (similar as in Adolphi & Muscheler, 2016).

A time-dependent change in ocean diffusivity was induced using 3 scenarios, as shown in Fig. 4b. The control scenario is set at 50% of the pre-industrial value. We induce an abrupt increase in ocean ventilation (to 80% of the pre-industrial value), an abrupt decrease (to 25%), or a sequence of both. The duration of the events is chosen to reflect changes in the NorthGRIP calcium record, while the transition time was set to 200 years.

Figure 4c shows that the effects of the perturbations in ocean diffusivity on $\Delta^{14}C$ span several tens of permille after detrending. Thus, any feature in the ^{14}C records that is in the proximity of an abrupt climate change and has a comparable duration is uncertain and should not be used for matching. On the other hand, Fig. 4e shows that short-term variations of the modelled $\Delta^{14}C$ signal are less affected by the diffusivity perturbation. At least in principle, signals exceeding 10-20‰ that are much shorter than the climatic transitions could be used for wiggle-matching, since Fig. 4f shows that the different ocean diffusivities scenarios affect the high-passed $\Delta^{14}C$ only within 2‰, hardly above measurement uncertainties.

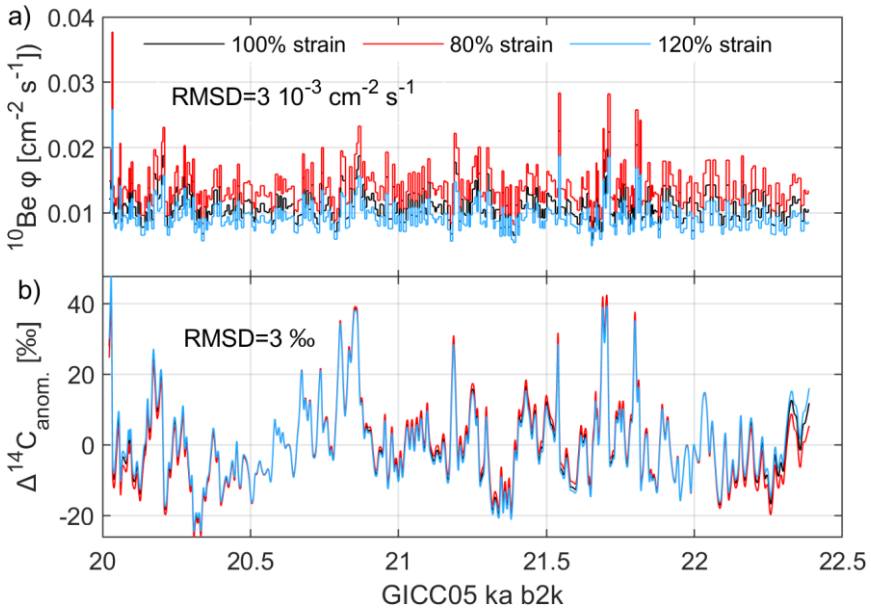

Figure 5 Sensitivity test of the effects of accumulation-related uncertainties on the carbon-cycle modelling. (a) Two strain-model scenarios produce different flux values. (b) The modelled $\Delta^{14}C$ curves are detrended, which largely removes the differences between the scenarios. However, the RMSD between the curves, 3‰, represents the remaining variability.

A second sensitivity test was performed to investigate the effect of accumulation uncertainties related to the strain model. We performed 2 experimental model runs where we shifted the thinning function (inverse strain) by ±20% of the mean value between 20 and 25 ka b2k, which is a realistic modelling uncertainty between independent studies of the accumulation rate (Rasmussen et al., 2014; Gkinis et al., 2014). Changing the strain rate creates an uncertainty of about 3‰ between the modelled and detrended $\Delta^{14}C$ curves, as shown in Fig. 5b. Furthermore, with a similar approach, we quantify the impact of ^{10}Be measurement uncertainty on the modelled $\Delta^{14}C$ to be 1‰ (Fig. S2). Adding these independent contributions in quadrature, we set an uncertainty for our modelled $\Delta^{14}C$ of 5‰. This uncertainty serves as an initial parameter for the wiggle-matching algorithm, described in the next

section; it furthermore agrees with the uncertainty adopted for the comparison of centennial variations of ^{14}C and ^{10}Be during the stable climate of the Holocene (Adolphi & Muscheler, 2016). However, as we have verified with our test, $\Delta^{14}C$ changes in the vicinity of climate perturbations bear a considerably higher uncertainty.

2.5 The wiggle-matching algorithm reproduced from Adolphi & Muscheler (2016) and its uncertainty

A wiggle-matching algorithm, adapted by Adolphi & Muscheler (2016) from the original formulation by Bronk Ramsey et al. (2001), represents an important tool for the quantification of offsets between time scales, along with visual inspection. The first input for the algorithm is the detrended $\Delta^{14}C$ modelled from the ice-core ^{10}Be. The second input is the detrended $\Delta^{14}C_{calcite}$ data from the Hulu Cave stalagmite samples. The output of the algorithm is a probability density of the time-scale offsets, $\vec{t}_{offset}$.

Following the approach by Adolphi & Muscheler (2016), we do not allow for stretching of the underlying chronologies. We investigated the offset probability within partially overlapping time windows $\overrightarrow{W}$, spaced every 50 years, obtaining a two-dimensional probability matrix $\boldsymbol{P}(\overrightarrow{W}, \vec{t}_{offset})$. We summarize the algorithm settings in the Method Appendix.

The most likely offset, $t^*_{offset}(\overrightarrow{W})$ is here defined as the maximum of $\boldsymbol{P}$. We identify the boundaries T1 and T2 between which $t^*_{offset}(\overrightarrow{W})$ is stable and we calculate an average offset.

After shifting each ice-core dataset by the proposed offset, we computed the χ^2 test between the $\Delta^{14}C$ curves. If the p-value was outside the 0.01-0.99 interval, we repeated the wiggle-matching using the standard deviation of the residuals (RMSD in ‰) as the uncertainty for the modelled $\Delta^{14}C$ curve. We re-evaluated the boundaries T1 and T2 and re-averaged the t^*_{offset} curves, obtaining a final estimation for the offset.

We aim to establish an uncertainty on the offset that considers the uncertainties of both ice cores and speleothems time-scales, as well as resolution limitations. We therefore applied a Monte-Carlo protocol to estimate the uncertainty and conducted the following steps:

1) For each modelled $\Delta^{14}C$ dataset and window W^*, we approximate the $\boldsymbol{P}(W^*, \vec{t}_{offset})$ as a Gaussian distribution, with 1σ as the average lower and upper width at half maximum of $\boldsymbol{P}(W^*, \vec{t}_{offset})$. By arbitrarily choosing the mode of **P** as the best offset, we can disregard any

other lobe of probability as spurious, with high confidence given by our visual inspection of the data.

2) For each dataset and window W^*, we sample randomly from the Gaussian for 10000 times to derive an ensemble of time-scale offsets;
3) By iterating steps 1 and 2 across all datasets and all windows within the established time boundaries T1 and T2, we compute the overall histogram of the sampled offsets;
4) We evaluate the 68% confidence interval of this histogram, around the best offset established as the mode.

This procedure is repeated separately for WD2014 and GICC05, and also for the Hulu H82 and MSD datasets. The algorithm is available in the Supplement.

3 Results

3.1 A promising inter-ice-core tie point for ^{10}Be synchronization

Previously used for the matching by Adolphi et al. (2018), a ^{10}Be increase at 21.7 ka b2k (GICC05 age) is visible in the new NorthGRIP data as well as in the WDC dataset (Fig. 2). This radionuclide increase resembles the ^{10}Be signal associated with the Maunder Solar Minimum (1645-1725 CE), which was a period of low solar activity and consequent increase in the global radionuclide production (Berggren et al., 2009; Eddy, 1976). In figure 6, we compare the Holocene and LGM counterparts of ^{10}Be at NorthGRIP finding similar shapes and duration. This supports the attribution of the ^{10}Be increase to a solar minimum during GS-2, which could explain the co-registration across $^{14}C_{calcite}$ and ^{10}Be datasets.

Based on the observed similarities in Fig. 6, we call the 21.7 ka b2k increase the "GS-2.1c ^{10}Be Event" (abbreviated *G2B event* in the following). To support the bipolar synchronization, after resampling the NorthGRIP ^{10}Be data on the resolution of WDC, we observe that the two ice cores register similar ^{10}Be amplitudes around the G2B event. The flux increases by 0.003 atoms cm^{-2} s^{-1} at both sites, which represents an increase of 40% and 30%, respectively, from the flux average values at NorthGRIP and WDC. The ^{10}Be concentration, on the other hand, increased only 30% (1.3 x 10^4 atoms/g) and 20% (0.9 x 10^4 atoms/g), respectively, from the concentration average values at NorthGRIP and WDC.

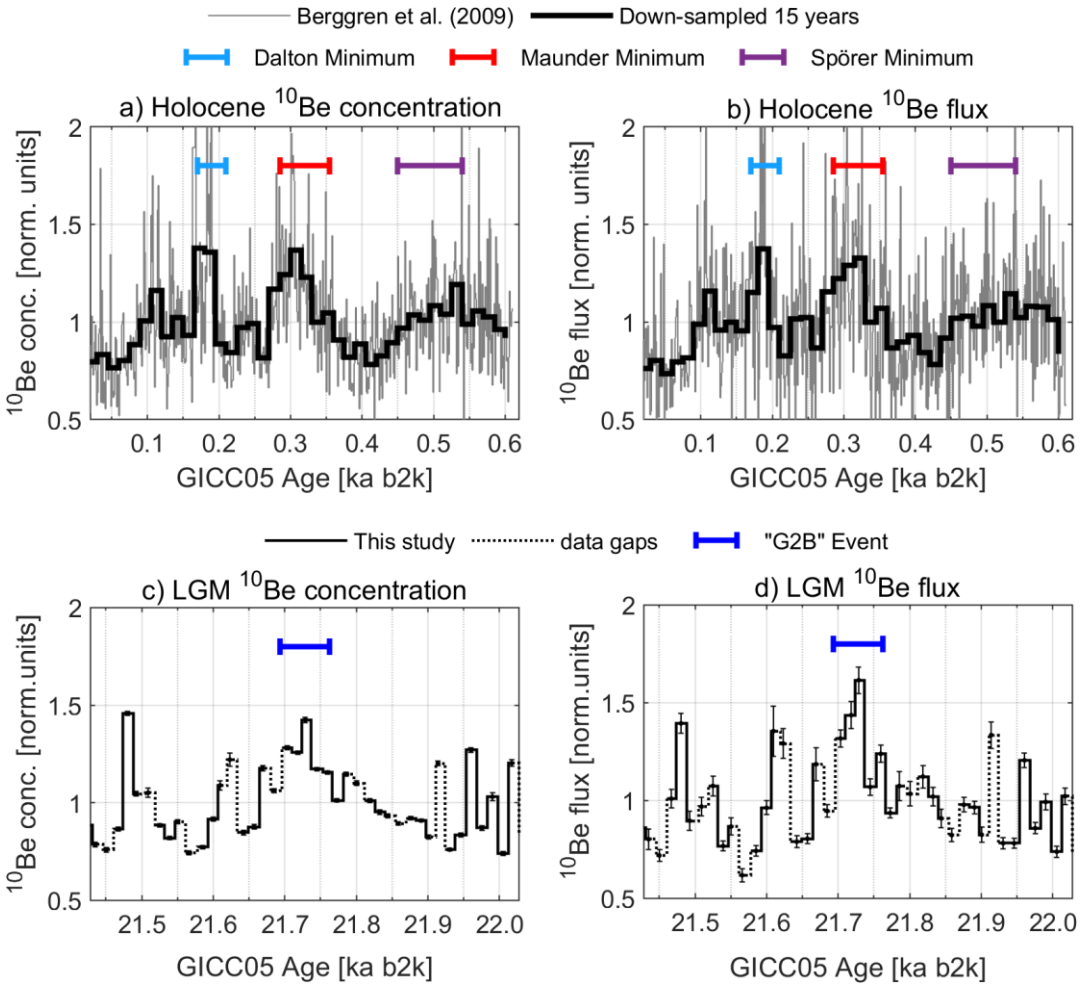

Figure 6 Comparison of ^{10}Be ice-core data in the Holocene, around the Maunder Minimum, and in the LGM, around the G2B event. Data was divided by the mean within ±300 years of the central event. (a, b) In the Holocene, the NorthGRIP ^{10}Be data by Berggren et al. (2009) compare well to the defined durations of the grand solar minima, which were independently recorded in the sunspot observations. An increase in the ^{10}Be production rate by about 40-50% from the average is produced by the solar minimum. The fluxes show a more abrupt increase in time, while concentrations record a more gradual increase. (c, d) In the LGM, the similarity of shape and duration to the Maunder Minimum supports the identification with a solar minimum.

3.2 Synchronization between ice cores using ^{10}Be

Having established the G2B event as a radionuclide production feature, we can synchronize Greenland ice cores by inserting new ^{10}Be tie points between NorthGRIP, GRIP, and GISP2. Furthermore, the G2B event can be used to improve the bipolar matching to Antarctica (Fig. 7).

We decided to compare the ^{10}Be data on similar resolutions to facilitate the identification of other common production features. Hence, we down-sampled the high-resolution data of NorthGRIP to the

same resolution as GRIP and WDC, since ice-core ^{10}Be measurements are averages over the sampling depth intervals and lose variability with decreasing resolution.

Table 2 ^{10}Be tie-point ages between NorthGRIP, GRIP, and WDC. The internal difference between the Greenland ice cores (δ) reaches 27 years at the G2B event. Likewise, the difference between WDC and NorthGRIP ages (Δ) indicates older ages for WDC at the G2B event and the youngest no. 4 tie point.

	GICC05 Age (years b2k)			WD2014 Age (years b2k)	
tie point	NorthGRIP	GRIP	δ	WDC	Δ(WDC-NorthGRIP)
4	20373	20370	3	20541	168±40
5	21372	21347	25		
6	21484	21458	26		
7 (G2B event)	21710	21683	27±21	21835	125±40
9	22383	22398	-15		
14	24119	24103	16		

Figure 7 shows the ^{10}Be concentrations from NorthGRIP, GRIP and WDC on their respective chronologies, together with a set of published tie points (Seierstad et al., 2014; Svensson et al., 2020). Between NorthGRIP and GRIP, we observe important similarities in the ^{10}Be data, which leads us to suggest 6 new ^{10}Be tie points: a peak at 20.4 ka b2k, a double peak at 21.5 ka b2k, the G2B event at 21.7 ka b2k, a single peak at 22.4 ka b2k, and a triple peak structure between 23.5 and 24.2 ka b2k. These tie points cover the previously tie-point-free section across GS-2.1b/c.

The tie points to WDC, of which Svensson et al. (2020) published the oldest (no. 15), is extended with the aid of two additional ^{10}Be tie points (no. 4 and no. 7/G2B). The choice of no. 4 as a bipolar tie point is motivated by a similar layer count of ~1300 years from G2B and a similar shape of the signals. The ages of the tie points are summarized in Table 2 and derived from the mid-depth of the highest peak.

The time scales of GRIP and NorthGRIP are slightly misaligned between 21 and 23 ka b2k by up to 27 years at the G2B event, probably due to the fact that GRIP ages were interpolated between widely spaced tie points. The uncertainty of this misalignment can be estimated as half the sum of the resolutions of NorthGRIP and GRIP measurements (± 21 years, 1 σ), as this is likely to limit our matching precision in each direction. Therefore, ^{10}Be measurements cannot be said to resolve matching issues between Greenland ice cores with very high precision, nonetheless we will use the new ^{10}Be tie points in the following to produce an updated accumulation rate for GRIP.

Furthermore, WD2014 and GICC05 are misaligned by 125±40 years at the G2B event, WD2014 being older; the uncertainty on this offset is given as half the sum of the resolutions of WDC and NorthGRIP data.

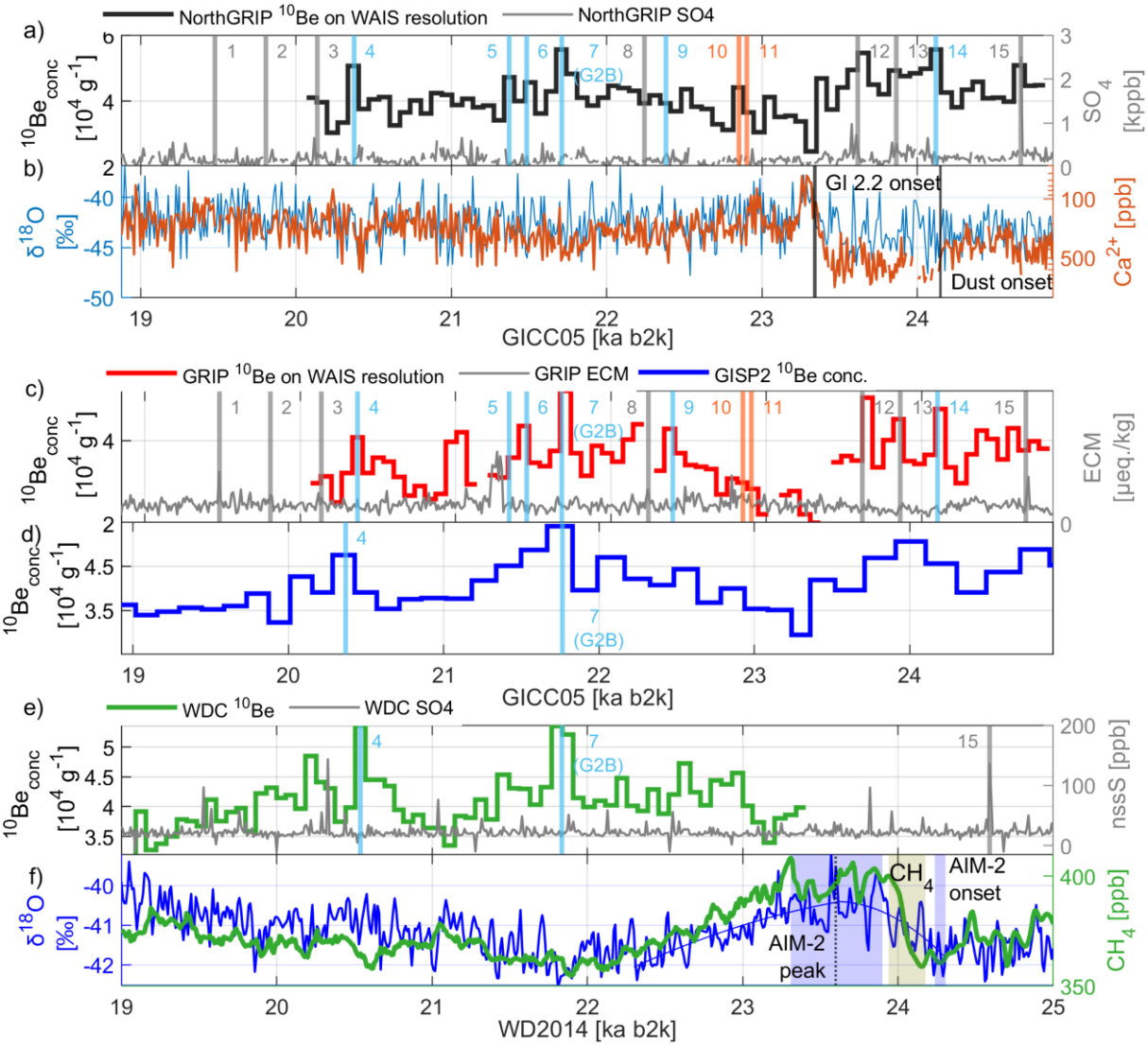

Figure 7 Bipolar tie points and climatic proxies. Vertical bars indicate the type of tie points (grey: volcanic, blue: ^{10}Be, orange: ammonium). The data were aligned using tie point 7 (G2B event), without stretching the chronologies. (a) The NorthGRIP tie points are based on ^{10}Be (black), sulfate data (grey) and ammonium data (not shown). (b) NorthGRIP $\delta^{18}O_{ice}$ and Ca^{2+} (inverted log-scale) qualitatively represent the climate in the LGM. (c) The GRIP tie points are based on ^{10}Be (red), ECM (grey), sulfate (not shown), ammonium (not shown). (d) The ^{10}Be data of GISP2 (blue) has a low resolution. Tie points no. 4 and 7 are however sufficiently visible in the data. (e) WDC ^{10}Be data (green) and nssS (grey; no. 15 by Svensson et al., 2020). (f) WDC climatic proxies, with CH_4 presented on the gas chronology by Buizert et al. (2015). The ages of the AIM-2 onset and peak and of the methane increase are described in the text.

The fact that the G2B event is 27 years older in NorthGRIP than GRIP means that the GRIP time scale and the accumulation rate need to be corrected, because the new tie points induced a change in the layer thickness. Hence, we calculated a new depth-depth interpolation between the two Greenland ice cores and we assigned an updated age scale to the GRIP depths.

The corrected accumulation of GRIP was computed by multiplying its layer thickness by a correction function of the relative change between the tie points. For example, since NorthGRIP has 1235 layers between tie-points nr. 4 and 7, while GRIP only has 1210 layers, the correction factor for the accumulation rate between these tie-points is 1.02. Due to these relatively small corrections, we do not find it necessary to apply any smoothing to the correction function. In the following, we denote fluxes of GRIP that were corrected in this way as "corrected fluxes" when we need to distinguish them from the previous version used by Adolphi et al. (2018). Although the effect of the accumulation correction is small, it has an impact on the amplitude of the G2B event signal in GRIP, making the NorthGRIP and GRIP modelled $\Delta^{14}C$ curves look more alike. At the resolution of the GISP2 data set, ^{10}Be appears to be sufficiently aligned around the G2B event and the peak at 20.4 ka b2k, hence no age correction was applied to GISP2.

In Figure 7, panels b and f, selected climatic proxies are shown to illustrate that a bipolar match across the LGM is already sufficient to change the timing between the two GIs and the AIM-2, bringing the AIM-2 to be closer to the GI-2.2 onset (a "before version" of the alignment of the climatic proxies is shown in Fig. 1).

In the WDC isotope data, we fit a curve to the $\delta^{18}O_{ice}$ record over the AIM-2 period to determine both the likely age for the onset of the warming slope and the peak – all on the original WD2014 chronology. We used the Matlab function 'WDC_breakpoint' provided by WAIS project members (2015), which fits the AIM with a double-polynomial fit to identify the maximum. However, the fit is sensitive to the starting guess for the position of the maximum; by varying the starting guess between 23 and 25 ka b2k, we observed that the fit finds several maxima. This fact is attributed to the shape of the signal being ambiguous and very broad. Moreover, a visual maximum of the AIM-2 is clearly identifiable at 23.6 ka b2k. Taking this as the central estimate, we estimate the location of the AIM-2 peak as 23600 ± 300 years b2k (1 σ). On the other hand, the onset of the AIM-2 is more easily defined to be 24272 ± 35 years b2k (1 σ).

The onset of the CH_4 increase at 24060 ± 118 (1σ) years b2k is defined as the instant at which the signal becomes higher (and remains higher) than 1 standard deviation from the average baseline of the period 24.5-25.5 ka b2k. The uncertainty of the CH_4 onset is quoted from the gas age uncertainty

of WD2014 (Fudge et al., 2017), which is mostly useful to compare CH_4 to the $\delta^{18}O_{ice}$ signal of the same ice core, WDC. All values are summarized in Table 3.

By aligning the two ice-core time scales at the G2B event, and without stretching the chronologies, we shift the GICC05 data by 125 years compared to WD2014 data. We observe that the AIM-2 peak now happens 125 years before the onset of GI-2.2, instead of 250 years before as was the case on the original time scales. The alignment at the G2B event is not sufficient to alter the order of the GI-2–AIM-2 sequence. What the new alignment shows is that the AIM-2 warming occurs within the dust peak and that the AIM-2 cooling occurs with the dust peak termination in Greenland, with potential influence of the GIs.

Table 3 Event onsets and terminations discussed in this work, corrected for the time-scale offsets, with 1σ confidence intervals. In the 'Original Calendar age' column, the onset of GIs and dust terminations are based on the original definition by Rasmussen et al. (2014) with reported uncertainties related to the event definition only. The dating uncertainty is dominated by the uncertainty of GICC05, which is about 600 years at this age. The ages of the AIM-2 and CH_4 increase in WDC were assessed as described in the main text. In the column 'Age according to wiggle-matching synchronization', GICC05 has been shifted by 375^{+250}_{-300} years, while the WD2014 ages were shifted by 225^{+200}_{-250} years, both towards older ages. The uncertainty on the new age was propagated from the original uncertainty and the offset uncertainty, using the asymmetric 1σ-boundaries of the offset.

Event	Archive	Age according to wiggle-matching synchronization (y b2k $^{+\sigma^+}_{-\sigma^-}$)	Original Calendar age (y b2k ± σ)
HS-2 onset	Hulu $\delta^{18}O_{calcite}$	24710 ± 40	24710 ± 40
Dust onset	NorthGRIP Ca^{2+}	$24525\ ^{+250}_{-300}$	24150±10
AIM-2 warming onset	$\delta^{18}O_{ice}$ WDC	24497^{+200}_{-250}	24272±35
Methane onset	WDC CH_4	$24285\ ^{+230}_{-270}$	24060±118
AIM-2 cooling onset	$\delta^{18}O_{ice}$ WDC	$23825\ ^{+360}_{-390}$	23600±300
Dust termination	NorthGRIP Ca^{2+}	23755^{+250}_{-300}	23380±20
Start of GI-2.2	$\delta^{18}O_{ice}$ Greenland	$23715\ ^{+250}_{-300}$	23340±20
Start of GS-2.2	$\delta^{18}O_{ice}$ Greenland	$23595\ ^{+250}_{-300}$	23220±20
Start of GI-2.1	$\delta^{18}O_{ice}$ Greenland	$23395\ ^{+250}_{-300}$	23020±20
Start of GS-2.1c	$\delta^{18}O_{ice}$ Greenland	$23275\ ^{+250}_{-300}$	22900±20

3.3 Carbon cycle modelling and wiggle-matching

Inspection of the measured $\Delta^{14}C_{calcite}$ (Fig. 8a) and the ^{10}Be-based $\Delta^{14}C$ (Fig. 8 b, c, e) confirms the expectation that a shift of the two ice-core chronologies towards older ages is required for a better alignment with the Hulu-cave $^{14}C_{calcite}$ record.

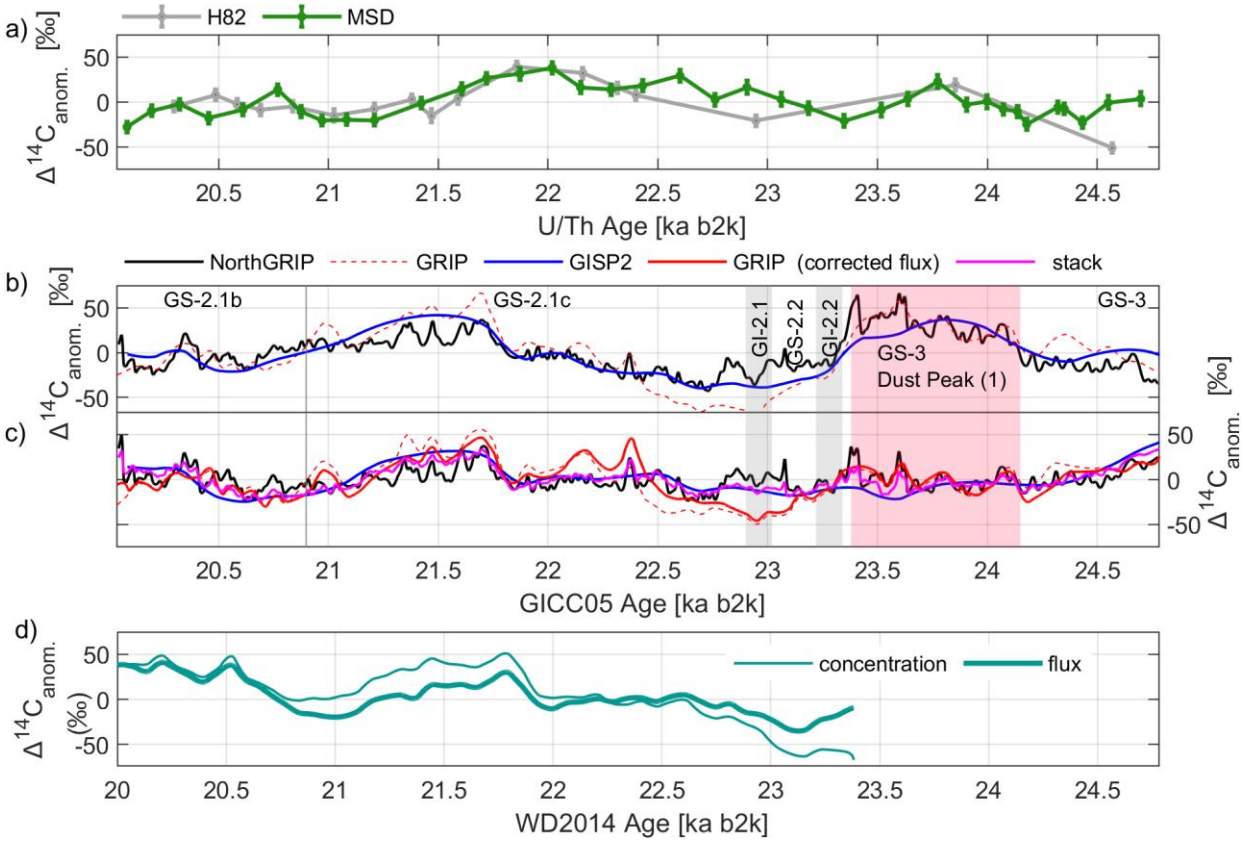

Figure 8 Carbon-cycle modelled $\Delta^{14}C$ compared to measured Hulu Cave data, before synchronization. (a) Hulu Cave $\Delta^{14}C_{calcite}$ (b) Modelled $\Delta^{14}C$ from Greenland ^{10}Be concentrations. (c) Modelled $\Delta^{14}C$ from Greenland ^{10}Be fluxes, including the flux stack (magenta). The effect of the flux correction of GRIP is mostly visible around the G2B event, where the corrected data (solid red line) shows a better agreement with the other cores. (d) $\Delta^{14}C$ modelled from WDC ^{10}Be fluxes and concentrations.

We observe two non-climatic tie-points between all $\Delta^{14}C$ curves:

1) The G2B event: a relatively abrupt increase of 30‰ in the modelled $\Delta^{14}C$ at 21.7 ka b2k (GICC05 ages). The most likely equivalent of this event is observed in the Hulu Cave data at around 22 ka b2k (U/Th ages), where an increase of about 25‰ happens abruptly between two data points which is followed by a slow decrease. In the H82 data by Southon et al. (2012), the increase is much less abrupt and spans 4 data points.
2) A 40‰ peak is observed in the ice-core $\Delta^{14}C$ at 20.4 ka b2k (GICC05). In Hulu Cave data, one elevated data point at 20.8 ka b2k (U/Th) is visible in the MSD dataset, but the H82 record does not show this peak.

We assume that the modelled and the measured $\Delta^{14}C$ should, after detrending, be dominated by the same production signal and that the differences we observe in the datasets can be explained by noise,

modelling uncertainties, and dynamics affecting the deposition rather than the production of the radionuclides. Therefore, we proceed with the wiggle-matching despite the observed differences.

Based on these considerations, we run the wiggle-matching algorithm exclusively in the 20.5-22.5 ka b2k range (U/Th ages), using data windows of 1300 years with an overlap of 50 years between successive windows. The 1300-year choice is motivated by a compromise between enough signal inclusion in each window and more precision, since preliminary tests showed that this value returned the most stable results, compared to windows of 1000 or 1500 years. For the U/Th time scale, we use both Hulu datasets but we separate our treatment for the H82 and the newer MSD data (Southon et al., 2012; Cheng et al., 2018), because of the different resolution and the slightly different signals recorded. For the WD2014 time scale, we use both the WDC ^{10}Be concentrations and fluxes, modelled to Δ^{14}C, since they are similar after carbon modelling. For the GICC05 time scale, we use all available Δ^{14}C modelled from concentrations, fluxes, and the flux stack, since they are similar at least around the production features we are going to match.

By averaging the obtained offset curves across the datasets and the interval (Fig. S4), we estimate the chronological offset to be 375years for GICC05 and 225 years for WD2014, using the MSD dataset exclusively. We do not give an uncertainty boundary for these offsets just yet, as we first perform a χ^2 test, following the protocol outlined in the Methods section. We evaluated the χ^2 and the associated p-value between each shifted Δ^{14}C curve and the Hulu dataset. For the flux-based datasets, the p-values were within the 0.01-0.99 threshold, except for the GRIP 'uncorrected' fluxes. This last exception motivates the exclusion of 'uncorrected' fluxes in the following, as we do not need to keep both GRIP flux-based curves, once we have ascertained that the 'corrected fluxes' satisfy our χ^2 test, possibly because of the improved chronological spacing of the samples.

In the case of all Greenlandic concentration-based curves, because of very low p-values of the χ^2 ($p<<0.01$), we decided to set the modelled-Δ^{14}C uncertainty to the RMSD of each dataset, which are between 12 and 21‰, less than the amplitude of the matched features. We repeat the wiggle-matching for these cases and base our offset estimation on the full Greenland dataset with the uncertainty method outlined above.

We therefore repeat the averaging of the time-scale offset (Fig. 9) between the MSD dataset and the GICC05 ensemble and we apply the Monte-Carlo iteration outlined in the Methods, between 21 and 22.1 ka b2k (the range highlighted in yellow in Fig. 9a, where edge effects can be avoided). We obtain the offset estimate of 375 years, a 68% confidence interval from 75 to 625 years, and a 95 % confidence interval from -300 to 1000 years. One assumption behind this approach is that the offset

should only change slowly with time, which is supported by the flatness of most curves in Fig. 9 (with some exception by the concentration-based offsets of NorthGRIP and GISP2).

For the WDC datasets, both flux- and concentration-based curves were shifted by 225 years. Upon performing the χ^2 test against the Hulu Cave data, the p-values were within the 0.01-0.99 tolerance interval, hence the uncertainty of the modelled $\Delta^{14}C$ data did not need to be re-evaluated. We compute the average time-scale offset (Fig. 9) between the MSD dataset and the WD2014 ensemble of flux and concentration-based curves and we apply the Monte-Carlo iteration outlined in the Methods, between 20.8 and 21.75 ka b2k (the range highlighted in yellow in Fig. 9b). We obtain the offset estimate of 225 years, a 68% confidence interval from -25 to 425 years, and a 95 % confidence interval from -350 to 750 years.

The difference between the ice-core offsets represents another indirect estimate of the offset between the Greenland and Antarctic chronologies, which in this way is determined to be 150 years, close to the offset of 125±33 years directly obtained by synchronizing the G2B event in the ^{10}Be fluxes.

Our result for GICC05 is smaller than the 550-year offset obtained by Adolphi et al. (2018) but fully consistent within the uncertainties of their estimate (95% probability interval: 215 – 670 years). For the H82 dataset, our analysis leads to offsets of about 500 ± 200 and 220 ± 500 years, for GICC05 and WD2014, respectively, which more closely reproduces the Adolphi et al. (2018) finding.

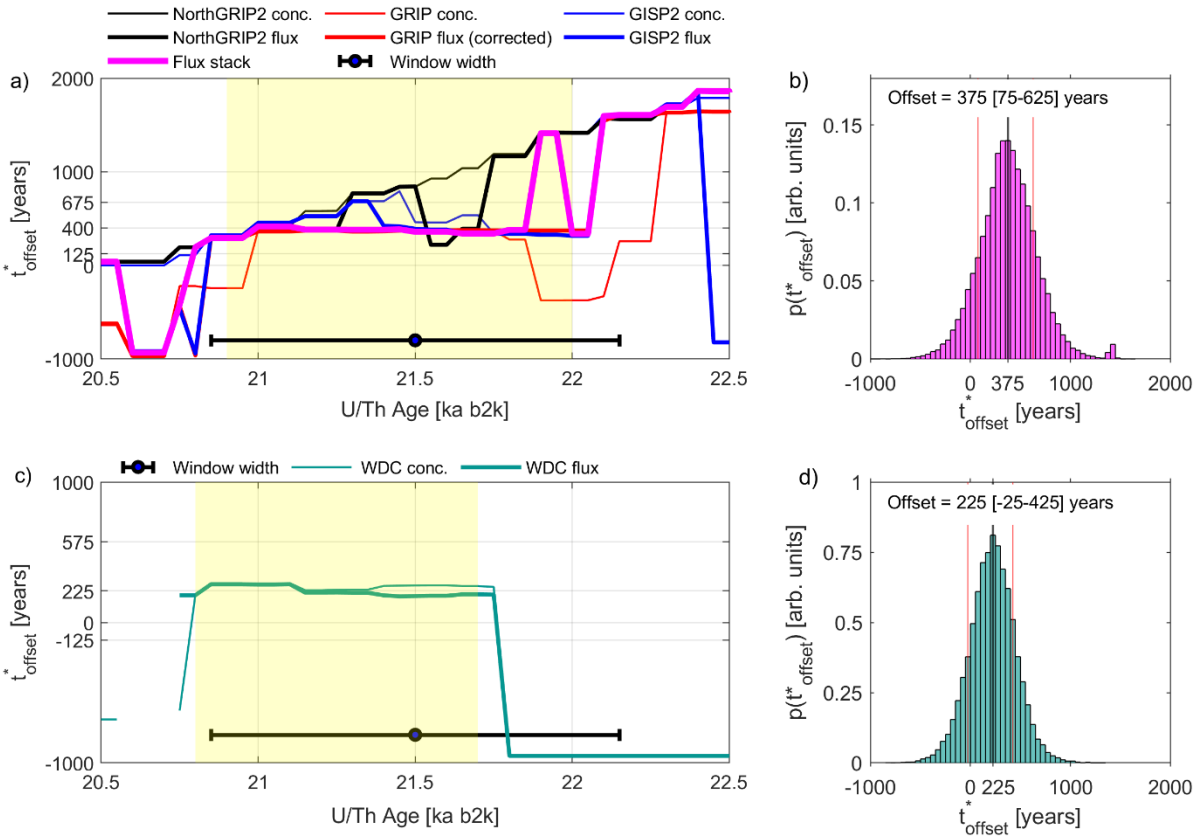

Figure 9 Wiggle-matching and Monte-Carlo results around the G2B event for Greenland (a, b) and the WDC core (b, c). Matlab code is provided in the Supplement. The curves in the left panels are the time-scale offset $t^*_{offset}(\vec{W})$ *of each ice-core dataset. The yellow area delimits the time intervals for averaging (T1 and T2), outside of which curve instability is caused by the lack of appropriate matching features in the data. (b) Distribution of the Greenland offset. From the histogram, we compute the 68% confidence interval of the offset (red lines). (d) Distribution of the WDC offset, with 68% confidence bars.*

4 Discussion

4.1 Climate compared after synchronization

In Figure 10 we show the radionuclide and climatic data after the synchronization proposed in section 3.3.

To reconstruct the sequence of events during the LGM, we need to estimate the onset and termination of HS-2. We suggest the onset of HS-2 to be defined by the $\delta^{18}O_{calcite}$ slope in Asian speleothems (Fig. 10b; Cheng et al., 2021). Here, we identify the onset of the HS-2 signal at Hulu Cave by the same methods used for the AIM-2, combining the WDC_breakpoint function with a Monte Carlo iteration. By averaging the onset in the two $\delta^{18}O_{calcite}$ onsets at Hulu Cave, one for each dataset, we obtain the HS-2 onset to be 24.71±0.04 ka b2k. This is earlier than, albeit compatible within 2 σ with

the definition by Li et al. (2021) of an HS-2 onset at around 24.48±0.08 ka b2k, based on another speleothem (Furong, China). The Hulu onset is also earlier than the Cherrapunji HS-2 onset at 24.47±0.04 ka b2k (Dong et al., 2022).

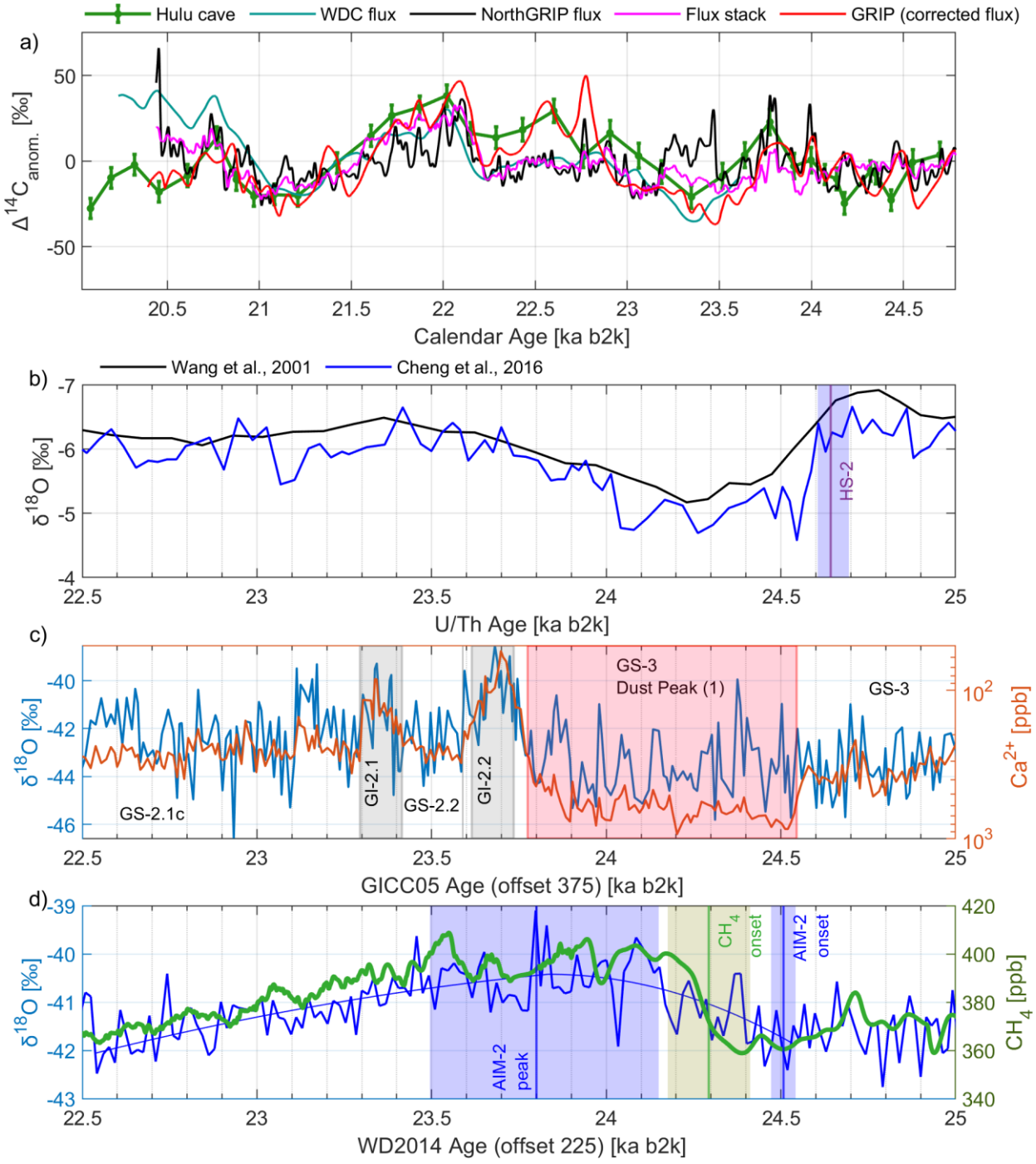

Figure 10 Radionuclide and climatic data after the synchronization. The Greenlandic records were shifted by 375 years towards older ages; the WDC records were shifted by 225 years towards older ages. (a) Radionuclide data used for wiggle matching plotted on the synchronized time scales. (b) Hulu-cave isotopes (reversed y-axis) highlight the suggested onset of HS-2 (Cheng et al., 2016). A lower-resolution dataset is also plotted for comparison (Wang et al., 2001). The termination of HS-2 is not defined, as multiple possibilities arise by comparing the two datasets. (c) Greenlandic proxy data on the shifted GICC05. (d) WDC proxy data on the shifted WD2014.

With the time-scale correction for WD2014, the onset of the AIM-2 warming occurs synchronously with the HS-2 onset, within the uncertainties determined both by the wiggle matching and by the AIM-2 fit. A delay could be expected given the centennial-scale response of Antarctic climate to Northern Hemisphere changes (Pedro et al., 2018; Svensson et al., 2020).

The AIM-2 maximum (i.e. the peak of $\delta^{18}O_{ice}$ in Antarctica) was here defined by considering only the data from WDC. By visual inspection, the peak of the AIM-2 signal could either be identified as two marked $\delta^{18}O_{ice}$ peaks at around 23.8 ka b2k (shifted WD2014 age) or as a prolonged plateau between 23.5 and 24.2 ka b2k. We observe that the 23.8 ka b2k peak in WDC occurs together with or slightly before GI-2.2, which is a similar result one obtains by merely synchronizing the data using the G2B event tie point (Fig. 7).

The shape of the AIM-2 signal differs across Antarctic ice cores (EPICA members, 2006), possibly because of registration differences across the continent. A comparative study of all Antarctic deep ice cores would improve our identification of the AIM-2, but the WD2014 timescale was only tied to few ice cores so far. At least, we can compare the recent South Pole ice core (SPICE), chronologically tied to the WD2014 (Winski et al., 2021). The shape of the AIM-2 in SPICE is similar to WDC (Fig. S5). While the onset occurs at the same age, the maximum is reached earlier in SPICE, at 24.1 ka b2k in the shifted WD2014 ages. This indicates that careful consideration of the geographic factors of the Antarctic continent are needed for an ultimate climate reconstruction of the AIM-2. In the meantime, we suggest that caution is exercised when interpreting minor isotopic signals.

The methane increase in WDC is registered ~210 years after the AIM-2 warming started and the HS-2 onset. This supports the theory by Rhodes et al. (2015) of an increased southern biogenic methane production as a delayed response to extreme northern-hemispheric cooling. The high methane levels appear to last between 460 and more than 1000 years, depending on how one defines the end of the methane plateau.

4.2 Discussion on causes of the offset for GICC05

In recent work by He et al. (2021), it was suggested that, although not reflected by Greenlandic water isotope records, a shutdown of the AMOC likely occurred during Heinrich Stadial 1, which was stronger than the AMOC shutdown of a 'regular' GS, producing a period of extreme winter cooling. They concluded that, rather than Greenland not experiencing any additional cooling during HS-1 (as proposed by Landais et al., 2018), the imprint of the cooling in the $\delta^{18}O_{ice}$ signal was cancelled by the effect of having less winter snow and by an increase of the $\delta^{18}O_{ice}$ level of summer snow, due to the first warming of the deglaciation. The flatness in the water isotope data is, in their analysis, the result of these counteracting effects of Greenland cooling: the HS-1-specific reduction in winter precipitation and the ^{18}O-enriched summer precipitation.

As far as the GICC05 layers are concerned, He et al. (2021) model a possible scenario over Greenland with a drastic decrease of winter precipitation by about 50% at the onset of HS-1. On the other hand, they predict the summer precipitation to increase steadily as the deglaciation progresses, which is largely unaffected by the AMOC shutdown. This could potentially have produced thin and irregular layers at the onset of HS-1, with the summer part of the layer gradually increasing over time.

Acknowledging the 125-year offset between GICC05 and WD2014 at 22 ka b2k, and the 375-year offset between GICC05 and the U/Th chronology, we proceed by discussing where the offset could have originated. According to Adolphi et al. (2018), the transfer function from GICC05 to IntCal is near to zero at 13 ka b2k, the closest tie-point younger than the G2B event. Occurring between these two time-horizons, the HS-1 period lasted from about 18 to 14.7 ka b2k, and is most often regarded as ending at the onset of GI-1. The authors of GICC05 retained the prior subdivision of the corresponding stadial, GS-2.1, in 3 sections (termed a, b, and c) of which GS-2.1a starts at 17.48 ka b2k and ends at the onset of GI-1 (Björck et al., 1998; Rasmussen et al., 2014). The onset of GS-2.1a was originally defined by a 2nd-order water isotope dip but occurs synchronously with an increase in the Greenland ice-core calcium profiles at roughly 17.6 – 17.4 ka b2k.

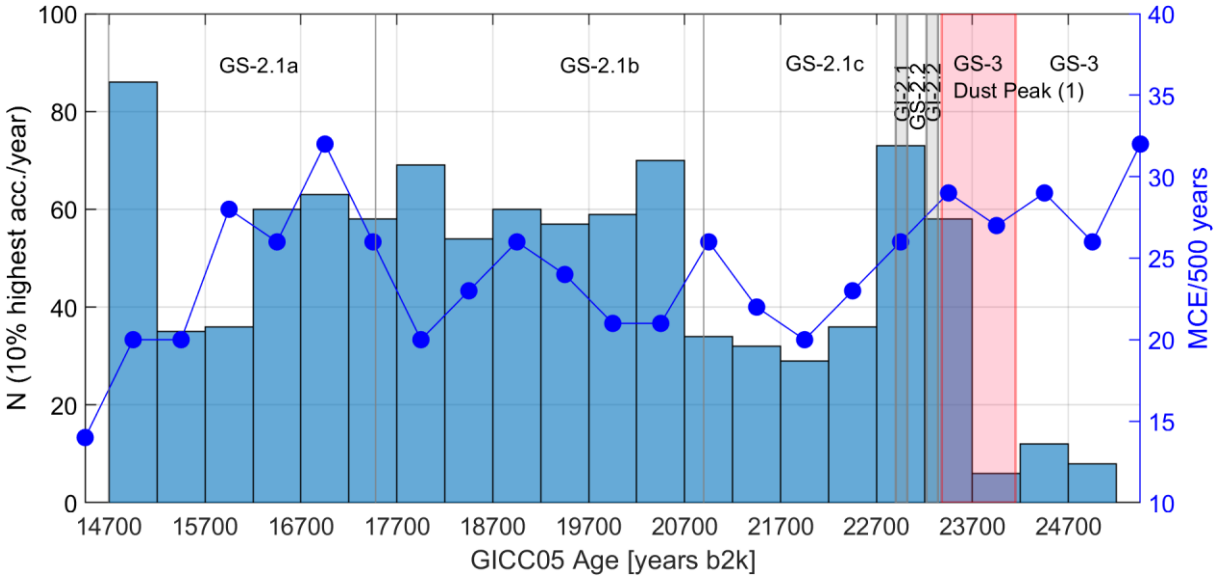

Figure 11 Highest accumulation years (histogram) and MCE (dark blue curve) based on the GICC05 time scale, computed on the same 500-years intervals.

If GICC05 missed a large number of annual layers across HS-1, the age of the onset of GS-2.1a would move towards older ages by a similar amount. We speculate that the onset of GS-2.1a could correspond to the onset of HE-1 (and thus the HS-1 period) and that calcium could be used as a signature of the change of atmospheric circulation influencing dust transport to Greenland during HS-1 as well as HS-2.

Part of the under-counted layers could have contributed to the uncertainty of GICC05. This was assessed by identifying so-called 'uncertain annual layers', that is, features that could be annual layers but are not clearly identified as such. Each uncertain layer contributed to the chronology and to the Maximum Counting Error (MCE) as 0.5±0.5 years (Rasmussen et al., 2006). Within GS-2.1a, the MCE grows by ~150 years, meaning that 300 uncertain layers were identified as 0.5±0.5 years. If we assume that all the uncertain annual layers in GS-2.1a were annual layers, an additional 150 years would appear in the chronology across this section.

As we have seen, according to He et al. (2021), a large number of very thin annual layers is a plausible scenario at least in the first part of HS-1, until the increasing summer precipitation alleviated the problem. As these layers are possibly unresolvable by the data, they would not be counted as uncertain layers, hence the MCE is probably not faithfully representing the full GICC05 uncertainty in sections where layer thicknesses are very small compared to the resolution of the data.

In addition to mis-assigned uncertain layers and layers missed altogether due to marginal data resolution, we here propose another explanation of what could have caused the under-count of

GICC05 layers. The layers that are on the higher end of the thickness distribution, even if they were classified as 'certain', might indicate where very low or absent winter precipitation could have made multiple annual layers appear as one.

To identify multiple layers, we highlight the years with highest accumulation in Fig. 11, where we also show the MCE, both per 500-year interval. The accumulation threshold is set at 0.09 m/year by integrating the highest 10% of the accumulation distribution between 14.7 and 25 ka b2k. The histogram in Fig. 11 thus shows the number of very thick layers in each time-bin.

The thickest layers across GS-2.1b and 2.1a have as many high-accumulation years as interstadial periods, which is surprising given that this period was very cold and had very low annual precipitation (Kindler et al., 2014).

For the MCE, observers of GICC05 encountered more issues at the onset of GS-2.1a, whereas the MCE stayed constant over the rest of GS-2.1. Hence, we suggest that a dating bias could have accumulated across GS-2.1a and GS-2.1b due to increased difficulty in identifying annual layers, caused by a weakening of the annual signal due to reduced amounts of winter snow. However, we find no clear evidence that this phenomenon occurs at the onset at HS-1 (17.7 ka b2k).

Recently, Dong et al. (2022) aligned the climate signature of HS-2 in the Cherrapunji speleothem to the calcium peak in Greenland, which was in turn aligned to Antarctica by one volcanic tie point at 24.6 ka b2k (match point no. 15 in Fig. 7; Svensson et al., 2020). Here, the GICC05 is 80 years older than WD2014, i.e. the offset has the opposite sign than at the G2B event. To produce such an inversion of the offset, an about 200 more layers had to be counted in NorthGRIP than in WDC over the interval between G2B and no. 15. However, a uniform stretching of GICC05 with respect to WD2014 is not advised, as we cannot assume that the offset is evenly distributed. A closer comparison via more bipolar volcanic tie points is needed to assess the time-varying nature of the offset.

4.3 Accuracy of the WD2014 and Hulu time scales during the LGM

For the WD2014 time scale, the offset can be compared to the uncertainties quoted for the chronology by Sigl et al. (2016). Between 20 and 25 ka b2k, 1σ uncertainties are between 100 and 125 years, which are smaller than the offset we find. This suggests that the authors of WD2014 may have underestimated their uncertainties, similar to GICC05, and that the layer counting in the glacial was also more challenging than acknowledged at first, but the two estimates are nonetheless within 2σ. However, the gradual warming recorded in Antarctica between 19 and 15 ka b2k (Pedro et al., 2011) likely did not lead to fast changes in the annual layers' expression. The WD2014 issues may thus be

mostly related to the low resolution of the data used for counting between 15 and 26 ka b2k (Sigl et al., 2016), which may have limited the accuracy of the chronology.

As a final remark, we have assumed here that the U/Th ages are correct and we have shifted the ice-core chronologies accordingly, on the basis of the challenging layer identification in the ice cores and of the small absolute uncertainties on the U/Th ages. However, the Hulu time scale could in principle also carry some error. For example, Corrick et al. (2020) speculate on possible issues with the Hulu chronology caused by interpolation and growth-rate modelling related to differences in the sample positioning for U/Th or $\delta^{18}O_{calcite}$ measurements. As we have seen above, there are at least two instances of Asian speleothems with a younger onset of HS-2 (Li et al. 2021; Dong et al. 2022), which agree with each other within their combined uncertainties. Apart from possible climatic delays across the speleothems, this could indicate issues in the absolute Hulu chronology, which would imply a smaller offset from the polar chronologies. Since, to our knowledge, there is no available radionuclide data for the Cherrapunji or Furong speleothem, our methodology relies on the Hulu $^{14}C_{calcite}$ record. It is crucial to resolve these differences in the speleothem chronologies as Hulu also forms the backbone of the ^{14}C-dating IntCal20 curve.

5 Conclusion

In this study, we have presented two new ^{10}Be datasets that allow both a bipolar synchronization and a comparison of polar climate to the Hulu speleothem archive during the 20-25 ka b2k period. The new NorthGRIP ^{10}Be dataset suggests a dating offset between GICC05 and U/Th time scales of 375^{+250}_{-300} years, which is less than the 550-year estimate by Adolphi et al. (2018), albeit consistent within uncertainties. Likewise, an offset was found between U/Th Hulu Cave dates and the WD2014 time scale of 225^{+200}_{-250} years, which is supported by the visual alignment of the datasets.

The rather large uncertainties on the time-scale offsets could be reduced in future studies. In terms of a bipolar match, a tight volcanic synchronization across the LGM, with the aid of our ^{10}Be match, would certainly link the two ice sheets with the most precision.

The issue of large uncertainties in the wiggle matching lies in resolution problems of the $^{14}C_{calcite}$, in the low signal-to-noise ratio of the G2B event, and in the carbon-cycle model likely not capturing every aspect of the LGM climate. The combination of these factors produces multiple possible alignments of our datasets. Therefore, higher-resolution ^{14}C data from absolutely-dated tree rings or from another speleothem, with a lower dead carbon fraction than Hulu, would improve our chances

to find reliable signal structures to match. From the ice-core side, high-resolution ^{10}Be from other ice cores would further limit the archive-specific and climate noise contributions.

In terms of the sequence of events between 20 and 25 ka b2k, the Greenlandic dust peak shifted to be roughly synchronous with the signal in the Hulu speleothem linked to the HS-2 onset. The onset of AIM-2 occurrs relatively near to the dust and Hulu signals, supporting the hypothesis that the AIM-2 warming is related to an AMOC shutdown during HS-2. The CH_4 increase onset in Antarctica also moved closer to the HS-2 onset, supporting the theory by Rhodes et al. (2015) of a long overlap of the methane plateau with the HS periods.

The termination of the Greenlandic dust peak and the almost synchronous onset of GI-2.2 were brought closer to the AIM-2 peak. We observe that the AIM-2 maximum, at least within WDC $\delta^{18}O_{ice}$ data, occurs together or before the GI-2.2 onset. This may indicate an exception to the average delay of 122±24 years found within other GI-AIM pairs, where the GI generally occurs before the AIM breakpoint (Svensson et al., 2020). Another piece of evidence suggests a deviation from the normal bipolar seesaw mechanism: It seems likely that the very brief GIs are not the primary cause of the sustained Antarctic gradual cooling taking place during the first millennia of the GS-2.1, but could be an indication that the AMOC resumed or gained more strength after GI-2.1 and into GS-2.1.

We investigated several possible reasons why the annual-layer counters of GICC05 could have missed annual layers across GS-2.1. We find that the MCE of GICC05 alone cannot account for all missing layers in the GS-2.1, but that either very thin annual layers or missing winter precipitation could have made it difficult, if not impossible, to identify the thinnest layers with the available data, and thus made the MCE estimation less robust.

6 Acknowledgement

G.S. and S.O.R. acknowledge support via the ChronoClimate project funded by the Carlsberg Foundation. S.O.R. also received support from the Villum Investigator Project IceFlow (grant no. 16572).

F.A. acknowledges support through the Helmholtz Association (grant VH-NG-1501). R.M. acknowledges support from the Swedish research council (grants DNR2013-8421 and DNR2018-05469).

K.W., T.W. and M.C. were supported by NSF grants 0839042 and 0839137. These authors acknowledge the support of the WAIS Divide Science Coordination Office at the Desert Research Institute in Reno, Nevada, for the collection and distribution of the WAIS Divide ice core (Kendrick

Taylor, NSF Grants 0440817 and 0230396), support from the NSF Office of Polar Programs, which funds the Ice Drilling Program; Raytheon Polar Services for logistics support in Antarctica; and the 109th New York Air National Guard for transport of equipment, people and ice cores in Antarctica. Finally, we acknowledge Geoff Hargreaves and his staff at the NSF Ice Core Facility, for archiving of the ice core and organizing and hosting ice core processing.

NGRIP was directed and organized by the Department of Geophysics at the Niels Bohr Institute for Astronomy, Physics and Geophysics, University of Copenhagen. It was supported by funding agencies in Denmark (SNF), Belgium (FNRS-CFB), France (IPEV and INSU/CNRS), Germany (AWI), Iceland (RannIs), Japan (MEXT), Sweden (SPRS), Switzerland (SNF) and the USA (NSF, Office of Polar Programs).

7 Data and Supplement

^{10}Be data of NorthGRIP and WDC are made available in the excel documents provided with the Supplement of this paper. Moreover, Matlab codes for reproducing Fig. 9 and Fig. 10a are provided in the Supplement, as well as the supplementary figures.

8 Methods Appendix

8.1 WDC measurements

Ice samples from the WAIS Divide ice core were stored and processed at the NSF Ice Core Facility in Lakewood, Colorado. Of each 1-m section from 2453-2599 m depth, a thin slice (DD-16) with a cross-section of ~2 cm^2 from the outside of the core was cut for ^{10}Be analysis and shipped in frozen form to Purdue University. For each ^{10}Be sample, two consecutive core sections were combined, yielding a total mass of 350-400 g per sample. Ice samples were weighed, melted, and acidified with a solution containing ~0.18 mg of Be carrier. The samples were passed through a 30 µm Millipore filter and loaded onto a 3 ml cation exchange column (Dowex 50WX8) from which the Be fraction was eluted and purified following established procedures (Finkel and Nishiizumi 1997; Woodruff et al. 2013). The Be fraction was precipitated as $Be(OH)_2$, transferred to a small quartz vial and heated in a tube furnace at 850 ºC. The BeO was mixed with Nb powder (Alfa Aesar, -325 mesh, Puratronic, 99.99%) and pressed into a stainless-steel cathode. The ^{10}Be/^{9}Be ratios of samples and blanks were measured by accelerator mass spectrometry at Purdue's PRIME laboratory

(Sharma et al. 2000), relative to well-documented $^{10}Be/Be$ AMS standards (Nishiizumi et al. 2007). The measured $^{10}Be/Be$ ratios of the samples were corrected for an average blank $^{10}Be/^{9}Be$ ratio of $(10 \pm 3) \times 10^{-15}$ which corresponds to typical blank corrections of 1-2% of the measured values. The blank-corrected $^{10}Be/^{9}Be$ ratios, combined with the sample mass and amount of Be carrier added yield ^{10}Be concentrations ranging from 3.1 to 5.4 x 10^4 atoms/g (Fig. 2d). Typical uncertainties (1σ) in the measured ^{10}Be concentrations are 1.5-3.5%. The measured ^{10}Be concentrations were not corrected for radioactive decay, which would increase all values by 1.0-1.2%.

8.2 NorthGRIP measurements

8.2.1 Ice cutting

At present, the required minimum weight for each ^{10}Be measurement is around 120 g. About half of the samples, in alternate order, had previously been cut in the shape sticks for gas measurements (section area of 3.5x3.5 cm^2), with a weight of around 600 g per bag (55 cm). The "gas sticks" were thus cut into 4 parts, resulting in pieces of 13.75 cm, corresponding to a resolution of about 7.5 years. The other half of the samples were cut from the archive piece to have a section area of ~2x3 cm^2. Each bag of these was then cut into two parts, hence each of such pieces weighs around 180 g and corresponds to about 14 years resolution. The campaign was performed with the necessity of keeping the total number of samples at around 320 for cost reasons. Since the total number of cut ice samples was 470, the pieces were selected to alternate between adjacent samples at 7.5 years resolution, to minimize the age gaps; the resulting ^{10}Be data consequently shows some data gaps.

8.2.2 Sample preparation and AMS Measurement (ETHZ)

Ice samples of 150-180 g were weighed and a solution containing 0.15 mg Be carrier (^{9}Be) was added, as well as 1 mg of Cl carrier. The samples were melted, not filtered, and run through cation exchange columns, from which the Be fraction was extracted. The melt water was further run through anion exchange columns to retain the chlorine content and stored for future ^{36}Cl measurement. The resulting $Be(OH)_2$ was heated in steps to 850° to obtain BeO and mixed with Niobium powder. Five blank samples of Milli-Q water were also measured for background assessment. More details about the most recent preparation protocol which is used at the Lund Laboratory can be found in Nguyen et al. (2021).

The $^{10}Be/^{9}Be$ ratios of the samples were measured in July 2020 at the AMS facilities at ETH in Zurich (Christl et al., 2013), where a total of 322 measurements were performed. Measured $^{10}Be/^{9}Be$ ratios

were normalized to the ETH Zurich in house standards S2007N and S2010N which in turn have been calibrated relative to primary standards provided by K. Nishiizumi (2007). An average blank correction of $^{10}Be/^{9}Be = 1.3 \pm 0.3\ 10^{-14}$ was applied to correct for ^{10}Be introduced with the Be-carrier. The blank correction corresponds to 2-3% of the measured ^{10}Be ratios. Calculated ^{10}Be concentrations range between 1.8 and 8.7 10^4 atoms/g and were decay corrected using a half-life of $1.387 \pm 0.016\ 10^6$ years, which, at these ages, produces a signal increase of only about 1%. The final uncertainties of the ^{10}Be concentrations were between 1 and 10 %.

8.3 From concentrations to fluxes

The concentration to flux conversion, for ice cores, is obtained by calculating $\varphi = \rho_{ice}\gamma\alpha$, where φ is the flux, γ is the ^{10}Be concentration, α is the accumulation rate, and ρ_{ice} is the ice density (0.917 g/cm^3).

8.4 Wiggle-matching algorithm settings

Thanks to the higher resolution of ice-core data with respect to Hulu data and thanks to the carbon-cycle model producing a continuous output, we approximate the ice-core modelled $\Delta^{14}C$ input as a continuous function of time, i.e. we resample it annually by linear interpolation. The second input, the Hulu-cave data, is a collection of discrete data points. The $\Delta^{14}C$ uncertainties are about 6‰ for the Hulu Cave data and 5‰ for the ice-core data. The datasets are detrended within each observation window before computing the probabilities. In particular, the ice-core $\Delta^{14}C$ is first shifted according to the scanned time offset, then detrended with respect to the observation window, and resampled to the Hulu-cave sampling points.

References

Adolphi, F., Muscheler, R., Svensson, A., Aldahan, A., Possnert, G., Beer, J., ... & Thieblemont, R. Persistent link between solar activity and Greenland climate during the Last Glacial Maximum. Nature Geoscience, 7(9), 662-666. https://doi.org/10.1038/ngeo2225 , 2014

Adolphi, F., & Muscheler, R. Synchronizing the Greenland ice core and radiocarbon time scales over the Holocene–Bayesian wiggle-matching of cosmogenic radionuclide records. Climate of the Past, 12(1), 15-30. https://doi.org/10.5194/cp-12-15-2016 , 2016

Adolphi, F., Bronk Ramsey, C., Erhardt, T., Edwards, R. L., Cheng, H., Turney, C. S., ... & Muscheler, R. Connecting the Greenland ice-core and U/ Th time scales via cosmogenic radionuclides: testing the synchroneity of Dansgaard–Oeschger events. Climate of the Past, 14(11), 1755-1781. https://doi.org/10.5194/cp-14-1755-2018 , 2018

Andersen, K. K., Svensson, A., Johnsen, S. J., Rasmussen, S. O., Bigler, M., Röthlisberger, R., ... & Clausen, H. B. The Greenland ice core chronology 2005, 15–42 ka. Part 1: constructing the time scale. Quaternary Science Reviews, 25(23-24), 3246-3257. https://doi.org/10.1016/j.quascirev.2006.08.002 , 2006

Bard, E., Rostek, F., Turon, J. L., & Gendreau, S. Hydrological impact of Heinrich events in the subtropical northeast Atlantic. Science, 289(5483), 1321-1324. DOI: 10.1126/science.289.5483.1321 , 2000

Bauska, T. K., Marcott, S. A., & Brook, E. J. Abrupt changes in the global carbon cycle during the last glacial period. Nature Geoscience, 14(2), 91-96. https://doi.org/10.1038/s41561-020-00680-2 , 2021

Berggren, A. M., Beer, J., Possnert, G., Aldahan, A., Kubik, P., Christl, M., ... & Vinther, B. M. A 600-year annual 10Be record from the NGRIP ice core, Greenland. Geophysical Research Letters, 36(11). https://doi.org/10.1029/2009GL038004 , 2009

Björck, S., Walker, M. J., Cwynar, L. C., Johnsen, S., Knudsen, K. L., Lowe, J. J., & Wohlfarth, B. An event stratigraphy for the Last Termination in the North Atlantic region based on the Greenland ice-core record: a proposal by the INTIMATE group. Journal of Quaternary Science: Published for the Quaternary Research Association, 13(4), 283-292. https://doi.org/10.1002/(SICI)1099-1417(199807/08)13:4<283::AID-JQS386>3.0.CO;2-A , 1998

Bronk Ramsey, C. B., van der Plicht, J., & Weninger, B. 'Wiggle matching'radiocarbon dates. Radiocarbon, 43(2A), 381-389. doi: 10.1017/S0033822200038248 , 2001

Buizert, C., Cuffey, K. M., Severinghaus, J. P., Baggenstos, D., Fudge, T. J., Steig, E. J., ... & Taylor, K. C. The WAIS Divide deep ice core WD2014 chronology–Part 1: Methane synchronization (68–31 ka BP) and the gas age–ice age difference. Climate of the Past, 11(2), 153-173. https://doi.org/10.5194/cp-11-153-2015 , 2015

Buizert, C., Sigl, M., Severi, M., Markle, B. R., Wettstein, J. J., McConnell, J. R., ... & Steig, E. J. Abrupt ice-age shifts in southern westerly winds and Antarctic climate forced from the north. Nature, 563(7733), 681-685. https://doi.org/10.1038/s41586-018-0727-5 , 2018

Cheng, H., Edwards, R. L., Sinha, A., Spötl, C., Yi, L., Chen, S., ... & Zhang, H. The Asian monsoon over the past 640,000 years and ice age terminations. nature, 534(7609), 640-646. http://dx.doi.org/10.1038/nature18591 , 2016

Cheng, H., Edwards, R. L., Southon, J., Matsumoto, K., Feinberg, J. M., Sinha, A., ... & Ning, Y. Atmospheric 14C/12C changes during the last glacial period from Hulu Cave. science, 362(6420), 1293-1297. DOI: 10.1126/science.aau0747 , 2018

Cheng, H., Xu, Y., Dong, X., Zhao, J., Li, H., Baker, J., ... & Edwards, R. L. Onset and termination of Heinrich Stadial 4 and the underlying climate dynamics. Communications Earth & Environment, 2(1), 1-11. https://doi.org/10.1038/s43247-021-00304-6 , 2021

Christl, M., Vockenhuber, C., Kubik, P. W., Wacker, L., Lachner, J., Alfimov, V., & Synal, H. A. The ETH Zurich AMS facilities: Performance parameters and reference materials. Nuclear Instruments and Methods in Physics Research Section B: Beam Interactions with Materials and Atoms, 294, 29-38. https://doi.org/10.1016/j.nimb.2012.03.004 , 2013

Corrick, E. C., Drysdale, R. N., Hellstrom, J. C., Capron, E., Rasmussen, S. O., Zhang, X., ... & Wolff, E. Synchronous timing of abrupt climate changes during the last glacial period. Science, 369(6506), 963-969. DOI: 10.1126/science.aay5538 , 2020

Dong, X., Kathayat, G., Rasmussen, S. O., Svensson, A., Severinghaus, J. P., Li, H., ... & Cheng, H. Coupled atmosphere-ice-ocean dynamics during Heinrich Stadial 2. Nature communications, 13(1), 5867. https://doi.org/10.1038/s41467-022-33583-4, 2022

Eddy, J. A. The Maunder Minimum: The reign of Louis XIV appears to have been a time of real anomaly in the behavior of the sun. Science, 192(4245), 1189-1202. DOI: 10.1126/science.192.4245.1189 , 1976

EPICA Community Members. One-to-one coupling of glacial climate variability in Greenland and Antarctica. Nature 444, 195–198 https://doi.org/10.1038/nature05301 , 2006

Erhardt, T., Bigler, M., Federer, U., Gfeller, G., Leuenberger, D., Stowasser, O., ... & Fischer, H. High resolution aerosol concentration data from the Greenland NorthGRIP and NEEM deep ice cores. Earth System Science Data Discussions, 1-25. https://doi.org/10.5194/essd-2021-324 , 2021

Finkel, R. C., & Nishiizumi, K. Beryllium 10 concentrations in the Greenland Ice Sheet Project 2 ice core from 3–40 ka. Journal of Geophysical Research: Oceans, 102(C12), 26699-26706. https://doi.org/10.1029/97JC01282 , 1997

Fudge, T. J., Markle, B. R., Cuffey, K. M., Buizert, C., Taylor, K. C., Steig, E. J., ... & Koutnik, M. Variable relationship between accumulation and temperature in West Antarctica for the past 31,000 years. Geophysical Research Letters, 43(8), 3795-3803. https://doi.org/10.1002/2016GL068356 , 2016

Fudge, T. J., & Fudge, T. J. WD2014: Time scale for WAIS Divide Core 2006 A (WDC-06A)" U.S. Antarctic Program (USAP) Data Center. https://doi.org/10.15784/60101 , 2017

Gkinis, V., Simonsen, S. B., Buchardt, S. L., White, J. W. C., & Vinther, B. M. Water isotope diffusion rates from the NorthGRIP ice core for the last 16,000 years–Glaciological and paleoclimatic implications. Earth and Planetary Science Letters, 405, 132-141. https://doi.org/10.1016/j.epsl.2014.08.022 , 2014

Guillevic, M., Bazin, L., Landais, A., Stowasser, C., Masson-Delmotte, V., Blunier, T., ... & Vinther, B. M. Evidence for a three-phase sequence during Heinrich Stadial 4 using a multiproxy approach based on Greenland ice core records. Climate of the Past, 10(6), 2115-2133. https://doi.org/10.5194/cp-10-2115-2014 , 2014

He, C., Liu, Z., Otto-Bliesner, B. L., Brady, E. C., Zhu, C., Tomas, R., ... & Severinghaus, J. P. Abrupt Heinrich Stadial 1 cooling missing in Greenland oxygen isotopes. Science advances, 7(25), eabh1007. DOI: 10.1126/sciadv.abh1007 , 2021

Heikkilä, U., Beer, J., Abreu, J. A., & Steinhilber, F. On the atmospheric transport and deposition of the cosmogenic radionuclides (10Be): A review. Space Science Reviews, 176(1), 321-332. https://doi.org/10.1007/s11214-011-9838-0 , 2013

Hughes, P. D., & Gibbard, P. L. A stratigraphical basis for the Last Glacial Maximum (LGM). Quaternary International, 383, 174-185. https://doi.org/10.1016/j.quaint.2014.06.006 , 2015

Hvidberg, C. S., Keller, K., Gundestrup, N. S., Tscherning, C. C., & Forsberg, R. Mass balance and surface movement of the Greenland Ice Sheet at Summit, Central Greenland. Geophysical research letters, 24(18), 2307-2310. https://doi.org/10.1029/97GL02280 , 1997

Johnsen, S. J., Clausen, H. B., Dansgaard, W., Gundestrup, N. S., Hammer, C. U., Andersen, U., ... & Fisher, D. The δ18O record along the Greenland Ice Core Project deep ice core and the problem of possible Eemian climatic instability. Journal of Geophysical Research: Oceans, 102(C12), 26397-26410. https://doi.org/10.1029/97GL02280 , 1997

Johnsen, S. J., Dahl-Jensen, D., Gundestrup, N., Steffensen, J. P., Clausen, H. B., Miller, H., ... & White, J. Oxygen isotope and palaeotemperature records from six Greenland ice-core stations: Camp Century, Dye-3, GRIP, GISP2, Renland and NorthGRIP. Journal of Quaternary Science: Published for the Quaternary Research Association, 16(4), 299-307. https://doi.org/10.1002/jqs.622 , 2001

Jones, T. R., Cuffey, K. M., White, J. W. C., Steig, E. J., Buizert, C., Markle, B. R., ... & Sigl, M. Water isotope diffusion in the WAIS Divide ice core during the Holocene and last glacial. Journal of Geophysical Research: Earth Surface, 122(1), 290-309. https://doi.org/10.1002/2016JF003938 , 2017

Köhler, P., Adolphi, F., Butzin, M., & Muscheler, R. Toward reconciling radiocarbon production rates with carbon cycle changes of the last 55,000 years. Paleoceanography and Paleoclimatology, 37(2), e2021PA004314. https://doi.org/10.1029/2021PA004314 , 2022

Landais, A., Capron, E., Masson-Delmotte, V., Toucanne, S., Rhodes, R., Popp, T., ... & Prié, F. Ice core evidence for decoupling between midlatitude atmospheric water cycle and Greenland temperature during the last deglaciation. Climate of the Past, 14(10), 1405-1415. https://doi.org/10.5194/cp-14-1405-2018 , 2018

Li, T. Y., Wu, Y., Shen, C. C., Li, J. Y., Chiang, H. W., Lin, K., ... & Edwards, R. L. High precise dating on the variation of the Asian summer monsoon since 37 ka BP. Scientific reports, 11(1), 1-14. https://doi.org/10.1038/s41598-021-88597-7 , 2021

Lin, J., Svensson, A., Hvidberg, C. S., Lohmann, J., Kristiansen, S., Dahl-Jensen, D., ... & Mulvaney, R. Magnitude, frequency and climate forcing of global volcanism during the last glacial period as seen in Greenland and Antarctic ice cores (60–9 ka). Climate of the Past Discussions, 1-45. https://doi.org/10.5194/cp-2021-100 , 2021

McManus, J. F., Francois, R., Gherardi, J. M., Keigwin, L. D., & Brown-Leger, S. Collapse and rapid resumption of Atlantic meridional circulation linked to deglacial climate changes. nature, 428(6985), 834-837. https://doi.org/10.1038/nature02494 , 2004

Muscheler, R., Beer, J., Wagner, G., & Finkel, R. C. Changes in deep-water formation during the Younger Dryas event inferred from 10Be and 14C records. Nature, 408(6812), 567-570. https://doi.org/10.1038/35046041 , 2000

Muscheler, R., Beer, J., Wagner, G., Laj, C., Kissel, C., Raisbeck, G. M., ... & Kubik, P. W. Changes in the carbon cycle during the last deglaciation as indicated by the comparison of 10Be and 14C records. Earth and Planetary Science Letters, 219(3-4), 325-340. https://doi.org/10.1016/S0012-821X(03)00722-2 , 2004

Muscheler, R. 14C and 10Be around 1650 cal BC:: are there contradictions between tree ring and ice core time scales?. Monographs of the Danish Institute at Athens (MoDIA), 10, 275-284. , 2009

Muscheler, R., Adolphi, F., & Knudsen, M. Assessing the differences between the IntCal and Greenland ice-core time scales for the last 14,000 years via the common cosmogenic radionuclide variations. Quaternary Science Reviews, 106, 81-87. http://dx.doi.org/10.1016/j.quascirev.2014.08.017 , 2014

Nguyen, L., Paleari, C. I., Müller, S., Christl, M., Mekhaldi, F., Gautschi, P., ... & Muscheler, R. The potential for a continuous 10Be record measured on ice chips from a borehole. Results in Geochemistry, 5, 100012. https://doi.org/10.1016/j.ringeo.2021.100012 , 2021

Nishiizumi, K., Imamura, M., Caffee, M. W., Southon, J. R., Finkel, R. C., & McAninch, J. Absolute calibration of 10Be AMS standards. Nuclear Instruments and Methods in Physics Research Section B: Beam Interactions with Materials and Atoms, 258(2), 403-413. https://doi.org/10.1016/j.nimb.2007.01.297 , 2007

North Greenland Ice Core Project members. High resolution record of Northern Hemisphere climate extending into the last interglacial period. Nature, 431(7005), 147-151. https://doi.org/10.1038/nature02805, 2004

Peck, V. L., Hall, I. R., Zahn, R., Elderfield, H., Grousset, F., Hemming, S. R., & Scourse, J. D. High resolution evidence for linkages between NW European ice sheet instability and Atlantic Meridional Overturning Circulation. Earth and Planetary Science Letters, 243(3-4), 476-488. https://doi.org/10.1016/j.epsl.2005.12.023 , 2006

Pedro, J. B., Van Ommen, T. D., Rasmussen, S. O., Morgan, V. I., Chappellaz, J., Moy, A. D., ... & Delmotte, M. The last deglaciation: timing the bipolar seesaw. Climate of the Past, 7(2), 671-683. https://doi.org/10.5194/cp-7-671-2011 , 2011

Pedro, J. B., Jochum, M., Buizert, C., He, F., Barker, S., & Rasmussen, S. O. Beyond the bipolar seesaw: Toward a process understanding of interhemispheric coupling. Quaternary Science Reviews, 192, 27-46. https://doi.org/10.1016/j.quascirev.2018.05.005, 2018

Raisbeck, G. M., Yiou, F., Fruneau, M., Loiseaux, J. M., Lieuvin, M., Ravel, J. C., & Lorius, C. Cosmogenic 10Be concentrations in Antarctic ice during the past 30,000 years. Nature, 292(5826), 825-826. https://doi.org/10.1038/292825a0 , 1981

Rasmussen, S. O., Andersen, K. K., Svensson, A. M., Steffensen, J. P., Vinther, B. M., Clausen, H. B., ... & Ruth, U. A new Greenland ice core chronology for the last glacial termination. Journal of Geophysical Research: Atmospheres, 111(D6). https://doi.org/10.1029/2005JD006079 , 2006

Rasmussen, S. O., Seierstad, I. K., Andersen, K. K., Bigler, M., Dahl-Jensen, D., & Johnsen, S. J. Synchronization of the NGRIP, GRIP, and GISP2 ice cores across MIS 2 and palaeoclimatic implications. Quaternary Science Reviews, 27(1-2), 18-28. https://doi.org/10.1016/j.quascirev.2007.01.016 , 2008

Rasmussen, S. O., Bigler, M., Blockley, S. P., Blunier, T., Buchardt, S. L., Clausen, H. B., ... & Winstrup, M. A stratigraphic framework for abrupt climatic changes during the Last Glacial period based on three synchronized Greenland ice-core records: refining and extending the INTIMATE event stratigraphy. Quaternary Science Reviews, 106, 14-28. https://doi.org/10.1016/j.quascirev.2014.09.007 , 2014

Reimer, P. J., Austin, W. E., Bard, E., Bayliss, A., Blackwell, P. G., Ramsey, C. B., ... & Talamo, S. The IntCal20 Northern Hemisphere radiocarbon age calibration curve (0–55 cal kBP). Radiocarbon, 62(4), 725-757. doi:10.1017/RDC.2020.41 , 2020

Rhodes, R. H., Brook, E. J., Chiang, J. C., Blunier, T., Maselli, O. J., McConnell, J. R., ... & Severinghaus, J. P. Enhanced tropical methane production in response to iceberg discharge in the North Atlantic. Science, 348(6238), 1016-1019. DOI: 10.1126/science.1262005 , 2015

Schüpbach, S., Fischer, H., Bigler, M., Erhardt, T., Gfeller, G., Leuenberger, D., ... & Wolff, E. W. Greenland records of aerosol source and atmospheric lifetime changes from the Eemian to the Holocene. Nature communications, 9(1), 1-10. https://doi.org/10.1038/s41467-018-03924-3 , 2018

Seierstad, I. K., Abbott, P. M., Bigler, M., Blunier, T., Bourne, A. J., Brook, E., ... & Vinther, B. M. Consistently dated records from the Greenland GRIP, GISP2 and NGRIP ice cores for the past 104 ka reveal regional millennial-scale δ18O gradients with possible Heinrich event imprint. Quaternary Science Reviews, 106, 29-46. https://doi.org/10.1016/j.quascirev.2014.10.032 , 2014

Sharma P., Bourgeois M., Elmore D., Granger D., Lipschutz M. E., Ma X., Miller T., Mueller K., Rickey F., Simms P. and Vogt S. RIME lab AMS performance, upgrades and research applications. Nuclear Instruments and Methods B172, 112-123. https://doi.org/10.1016/S0168-583X(00)00132-4 , 2000

Siegenthaler, U. Uptake of excess CO2 by an outcrop-diffusion model of the ocean. Journal of Geophysical Research: Oceans, 88(C6), 3599-3608. https://doi.org/10.1029/JC088iC06p03599 , 1983

Sigl, M., Fudge, T. J., Winstrup, M., Cole-Dai, J., Ferris, D., McConnell, J. R., ... & Sowers, T. A. The WAIS Divide deep ice core WD2014 chronology–Part 2: Annual-layer counting (0–31 ka BP). Climate of the Past, 12(3), 769-786. https://doi.org/10.5194/cp-12-769-2016 , 2016

Southon, J., Noronha, A. L., Cheng, H., Edwards, R. L., & Wang, Y. A high-resolution record of atmospheric 14C based on Hulu Cave speleothem H82. Quaternary Science Reviews, 33, 32-41. https://doi.org/10.1016/j.quascirev.2011.11.022 , 2012

Steinhilber, F., Abreu, J. A., Beer, J., Brunner, I., Christl, M., Fischer, H., ... & Wilhelms, F. 9,400 years of cosmic radiation and solar activity from ice cores and tree rings. Proceedings of the National Academy of Sciences, 109(16), 5967-5971. https://doi.org/10.1073/pnas.1118965109 , 2012

Stocker, T. F., & Johnsen, S. J. A minimum thermodynamic model for the bipolar seesaw. Paleoceanography, 18(4). https://doi.org/10.1029/2003PA000920 , 2003

Stuiver, M., & Polach, H. A. Discussion reporting of 14C data. Radiocarbon, 19(3), 355-363. doi:10.1017/S0033822200003672 , 1977

Stuiver, M., & Grootes, P. M. GISP2 oxygen isotope ratios. Quaternary Research, 53(3), 277-284. doi:10.1006/qres.2000.2127 , 2000

Svensson, A., Andersen, K. K., Bigler, M., Clausen, H. B., Dahl-Jensen, D., Davies, S. M., ... & Vinther, B. M. A 60 000 year Greenland stratigraphic ice core chronology. Climate of the Past, 4(1), 47-57. https://doi.org/10.5194/cp-4-47-2008 , 2008

Svensson, A., Dahl-Jensen, D., Steffensen, J. P., Blunier, T., Rasmussen, S. O., Vinther, B. M., ... & Bigler, M. Bipolar volcanic synchronization of abrupt climate change in Greenland and Antarctic ice cores during the last glacial period. Climate of the Past, 16(4), 1565-1580. https://doi.org/10.5194/cp-16-1565-2020 , 2020

Wagner, G., Beer, J., Masarik, J., Muscheler, R., Kubik, P. W., Mende, W., ... & Yiou, F. Presence of the solar de Vries cycle (~ 205 years) during the last ice age. Geophysical Research Letters, 28(2), 303-306. https://doi.org/10.1029/2000GL006116 , 2001

WAIS Divide Project Members. Precise interpolar phasing of abrupt climate change during the last ice age. Nature, 520(7549), 661-665. https://doi.org/10.1038/nature14401 , 2015

Wang, Y. J., Cheng, H., Edwards, R. L., An, Z. S., Wu, J. Y., Shen, C. C., & Dorale, J. A. A high-resolution absolute-dated late Pleistocene monsoon record from Hulu Cave, China. Science, 294(5550), 2345-2348. DOI: 10.1126/science.1064618 , 2001

Winski, D. A., Fudge, T. J., Ferris, D. G., Osterberg, E. C., Fegyveresi, J. M., Cole-Dai, J., ... & McConnell, J. R. The SP19 chronology for the South Pole Ice Core–Part 1: volcanic matching and annual layer counting. Climate of the Past, 15(5), 1793-1808. https://doi.org/10.5194/cp-15-1793-2019, 2019

Woodruff T. E., Welten K. C., Caffee M. W. and Nishiizumi K. nterlaboratory comparison of 10Be concentrations in two ice cores from Central West Antarctica. Nuclear Instruments and Methods in Physics Research, B294, 77–80. https://doi.org/10.1016/j.nimb.2012.08.033 , 2013

Wu, J., Wang, Y., Cheng, H., & Edwards, L. R. An exceptionally strengthened East Asian summer monsoon event between 19.9 and 17.1 ka BP recorded in a Hulu stalagmite. Science in China Series D: Earth Sciences, 52(3), 360-368, https://doi.org/10.1007/s11430-009-0031-1, 2009

Yiou, F., Raisbeck, G. M., Baumgartner, S., Beer, J., Hammer, C., Johnsen, S., ... & Yiou, P. Beryllium 10 in the Greenland ice core project ice core at summit, Greenland. Journal of Geophysical Research: Oceans, 102(C12), 26783-26794. https://doi.org/10.1029/97JC01265 , 1997

Zheng, M., Sturevik-Storm, A., Nilsson, A., Adolphi, F., Aldahan, A., Possnert, G., & Muscheler, R. Geomagnetic dipole moment variations for the last glacial period inferred from cosmogenic radionuclides in Greenland ice cores via disentangling the climate and production signals. Quaternary Science Reviews, 258, 106881, https://doi.org/10.1016/j.quascirev.2021.106881, 2021